Supplementary Appendix

NCBP2-mediated apoptosis contributes to developmental defects of the schizophrenia-associated 3q29 deletion

Mayanglambam Dhruba Singh[1*], Matthew Jensen[1*], Micaela Lasser[2], Emily Huber[1], Tanzeen Yusuff[1], Lucilla Pizzo[1], Brian Lifschutz[1], Inshya Desai[1], Alexis Kubina[1], Sneha Yennawar[1], Sydney Kim[2], Janani Iyer[1], Diego E. Rincon-Limas[3], Laura Anne Lowery[2], and Santhosh Girirajan[1,4]

Table of Contents

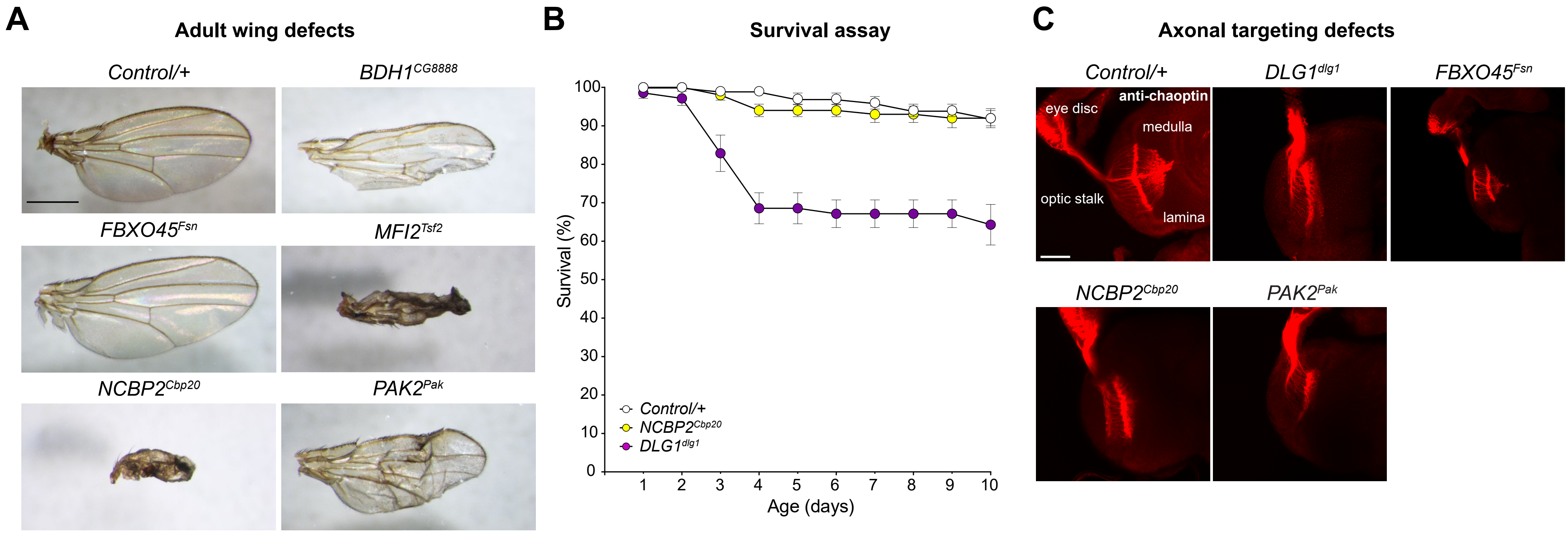
A
Adult wing defects
Control/+
BDH1^CG8888
FBXO45^Fsn
MFI2^Tsf2
NCBP2^Cbp20
PAK2^Pak
B
Survival assay
Survival (%)
Age (days)
Control/+
NCBP2^Cbp20
DLG1^dlg1
C
Axonal targeting defects
Control/+
DLG1^dlg1
FBXO45^Fsn
anti-chaoptin
eye disc
medulla
optic stalk
lamina
NCBP2^Cbp20
PAK2^Pak

Figure S1. Developmental defects in flies with tissue-specific knockdown of individual 3q29 homologs. (A) Adult flies with pan-neuronal knockdown of *DLG1*^{dlg1} showed approximately 30% lethality between days 1-4 (one-way ANOVA, $p=1.09\times10^{-10}$, df = 1, F = 77.093), which was not observed in control or *NCBP2*^{Cbp20} flies. Data represented shows mean ± standard deviation of 10 independent groups of 10 flies for each homolog. **(B)** Images of adult fly wings (scale bar = 500um) show a range of phenotypic defects due to wing-specific knockdown of individual 3q29 homologs. **(C)** Representative confocal images of larval eye discs stained with anti-chaoptin (scale bar = 30 µm) illustrate defects in axonal targeting from the retina to the optic lobes of the brain upon eye-specific knockdown of individual 3q29 homologs.

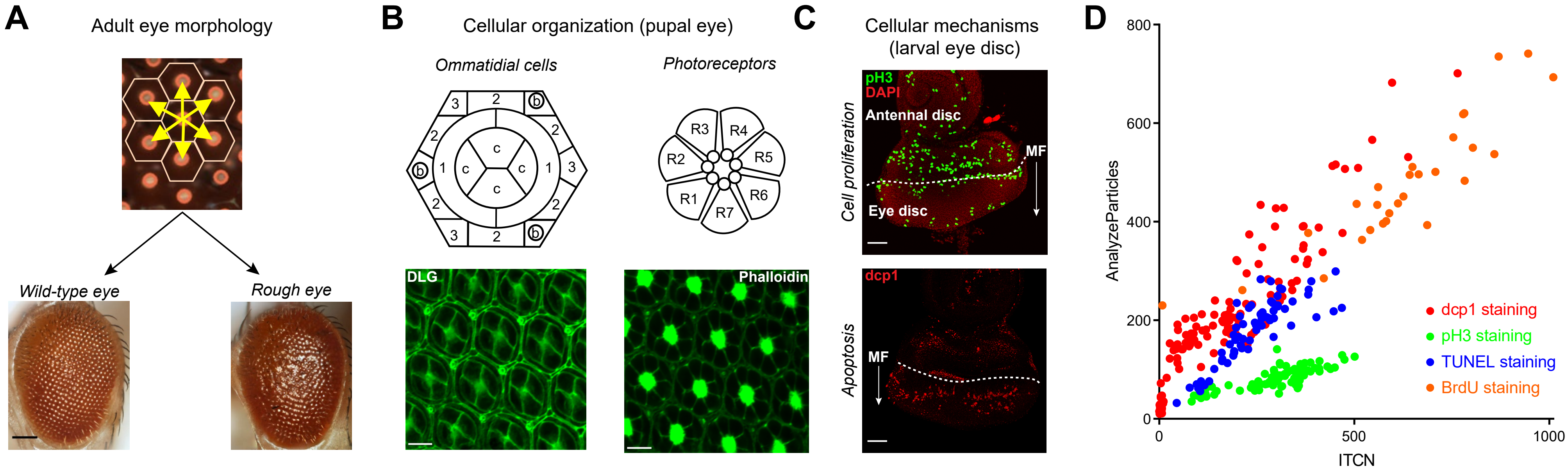

A
Adult eye morphology
Wild-type eye
Rough eye
B
Cellular organization (pupal eye)
Ommatidial cells
Photoreceptors
DLG
Phalloidin
C
Cellular mechanisms (larval eye disc)
Cell proliferation
pH3
DAPI
Antennal disc
Eye disc
MF
Apoptosis
dcp1
D
AnalyzeParticles
ITCN
dcp1 staining
pH3 staining
TUNEL staining
BrdU staining

Figure S2. Examination of cellular phenotypes in the *Drosophila* eye. We tested individual and pairwise knockdown of 3q29 homologs for cellular phenotypes in the adult, pupal and larval eyes. **(A)** We first used the *Flynotyper* software (1) to quantify the degree of ommatidial disorganization leading to rough eye phenotypes in adult flies, as represented by the distance and angles between adjacent ommatidia (yellow arrows). **(B)** We next stained pupal eyes with anti-DLG to observe changes in the number and arrangement of ommatidial cells, including cone cells (c), bristle cells (b), and primary, secondary and tertiary cells (1,2,3). We also examined the organization of the photoreceptor cells (R1-R7, with R8 not visible) in each ommatidia by staining the pupal eyes with Phalloidin. **(C)** We finally stained larval eye discs with markers of cellular processes, such as pH3 for proliferating cells and dcp1 for apoptosis. As the migration of the morphogenetic furrow (MF) across the larval eye discs leads to proliferation and differentiation of photoreceptor neurons (2), we examined changes in the number of stained cells posterior to the MF. **(D)** Scatter plot of cell counts in larval eye discs for dcp1, pH3, TUNEL, and BrdU-positive cells from 3q29 knockdown experiments quantified using two ImageJ plugins, AnalyzeParticles and Image-based Tool for Counting Nuclei (ITCN). As the two methods showed a strong correlation with each other (Pearson correlation, $n=285$, $r=0.736$, $p<2.2\times10^{-16}$), we used ITCN counts to display cell count data in the manuscript.

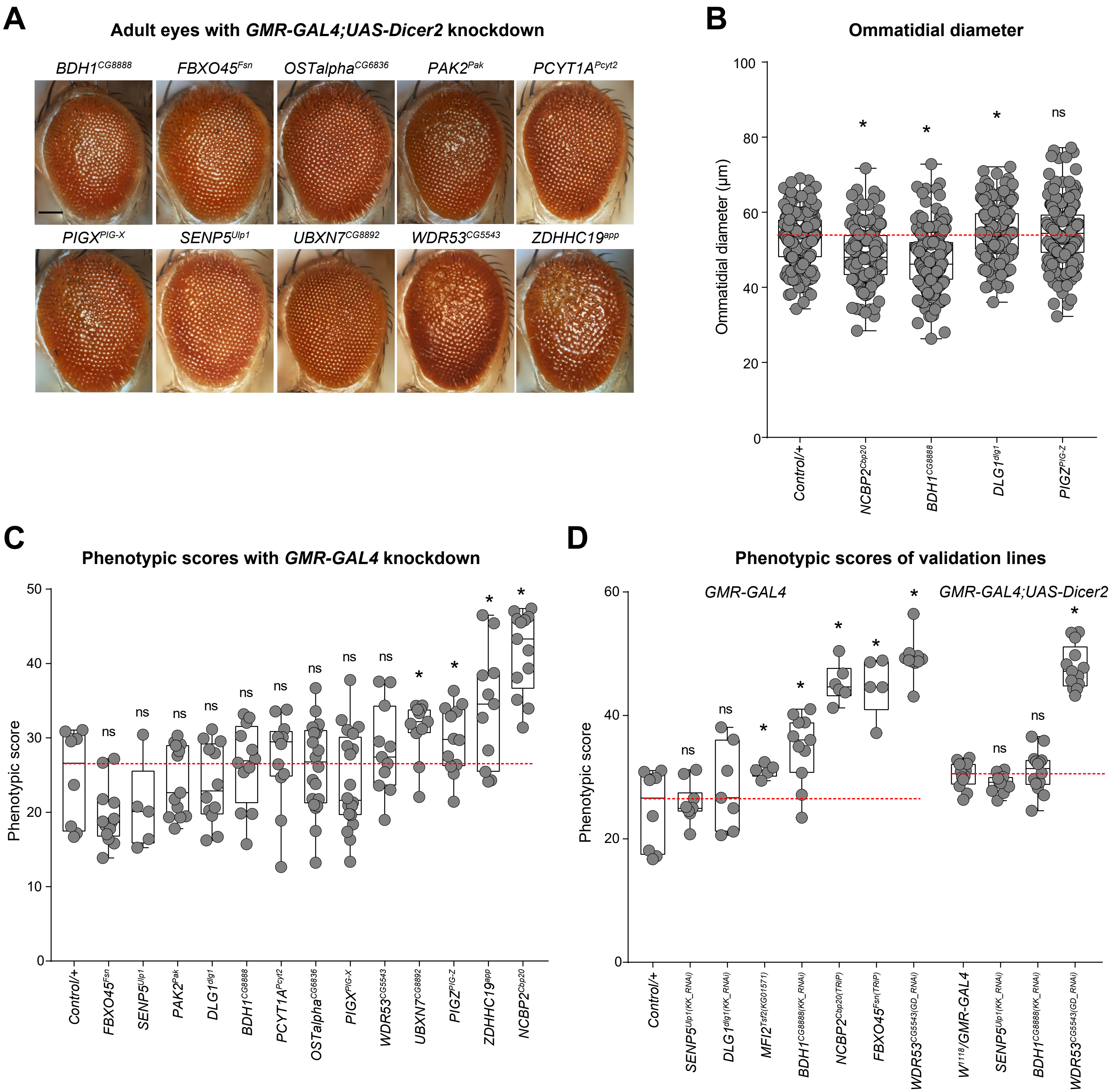

A
Adult eyes with GMR-GAL4;UAS-Dicer2 knockdown
$BDH1^{CG8888}$
$FBXO45^{Fsn}$
$OSTalpha^{CG6836}$
$PAK2^{Pak}$
$PCYT1A^{Pcyt2}$
$PIGX^{PIG-X}$
$SENP5^{Ulp1}$
$UBXN7^{CG8892}$
$WDR53^{CG5543}$
$ZDHHC19^{app}$
B
Ommatidial diameter
Ommatidial diameter (μm)
0
20
40
60
80
100
*
*
*
ns
Control/+
$NCBP2^{Cbp20}$
$BDH1^{CG8888}$
$DLG1^{dlg1}$
$PIGZ^{PIG-Z}$
C
Phenotypic scores with GMR-GAL4 knockdown
Phenotypic score
0
10
20
30
40
50
ns
ns
ns
ns
ns
ns
ns
ns
ns
*
*
*
*
Control/+
$FBXO45^{Fsn}$
$SENP5^{Ulp1}$
$PAK2^{Pak}$
$DLG1^{dlg1}$
$BDH1^{CG8888}$
$PCYT1A^{Pcyt2}$
$OSTalpha^{CG6836}$
$PIGX^{PIG-X}$
$WDR53^{CG5543}$
$UBXN7^{CG8892}$
$PIGZ^{PIG-Z}$
$ZDHHC19^{app}$
$NCBP2^{Cbp20}$
D
Phenotypic scores of validation lines
GMR-GAL4
GMR-GAL4;UAS-Dicer2
Phenotypic score
0
20
40
60
ns
ns
*
*
*
*
*
*
ns
ns
*
Control/+
$SENP5^{Ulp1(KK\_RNAi)}$
$DLG1^{dlg1(KK\_RNAi)}$
$MFI2^{Tsf2(KG01571)}$
$BDH1^{CG8888(KK\_RNAi)}$
$NCBP2^{Cbp20(TRiP)}$
$FBXO45^{Fsn(TRiP)}$
$WDR53^{CG5543(GD\_RNAi)}$
$W^{1118}/GMR\text{-}GAL4$
$SENP5^{Ulp1(KK\_RNAi)}$
$BDH1^{CG8888(KK\_RNAi)}$
$WDR53^{CG5543(GD\_RNAi)}$

Figure S3. Phenotypic screening for flies with eye-specific knockdown of individual 3q29 homologs. **(A)** Representative brightfield adult eye images of flies with knockdown of individual 3q29 homologs with *GMR-GAL4;UAS-Dicer2* (scale bar = 100 µm) show a wide range of phenotypic severity. **(B)** Box plot of ommatidial diameter in 3q29 single-hit knockdown flies with *GMR-GAL4* (n = 177–252 ommatidia, *$p < 0.05$, two-tailed Mann–Whitney test). **(C)** Box plot of phenotypic scores derived from *Flynotyper* for eye-specific knockdown of 13 individual homologs of 3q29 genes with *GMR-GAL4* (n = 5–20, *$p < 0.05$, one-tailed Mann–Whitney test). **(D)** Box plot of phenotypic scores derived from *Flynotyper* for eye-specific knockdown of 10 validation lines for homologs of 3q29 genes with *GMR-GAL4;UAS-Dicer2* (left) and *GMR-GAL4* (right) (n = 5–14, *$p < 0.05$, one-tailed Mann–Whitney test). All boxplots indicate median (center line), 25th and 75th percentiles (bounds of box), and minimum and maximum (whiskers).

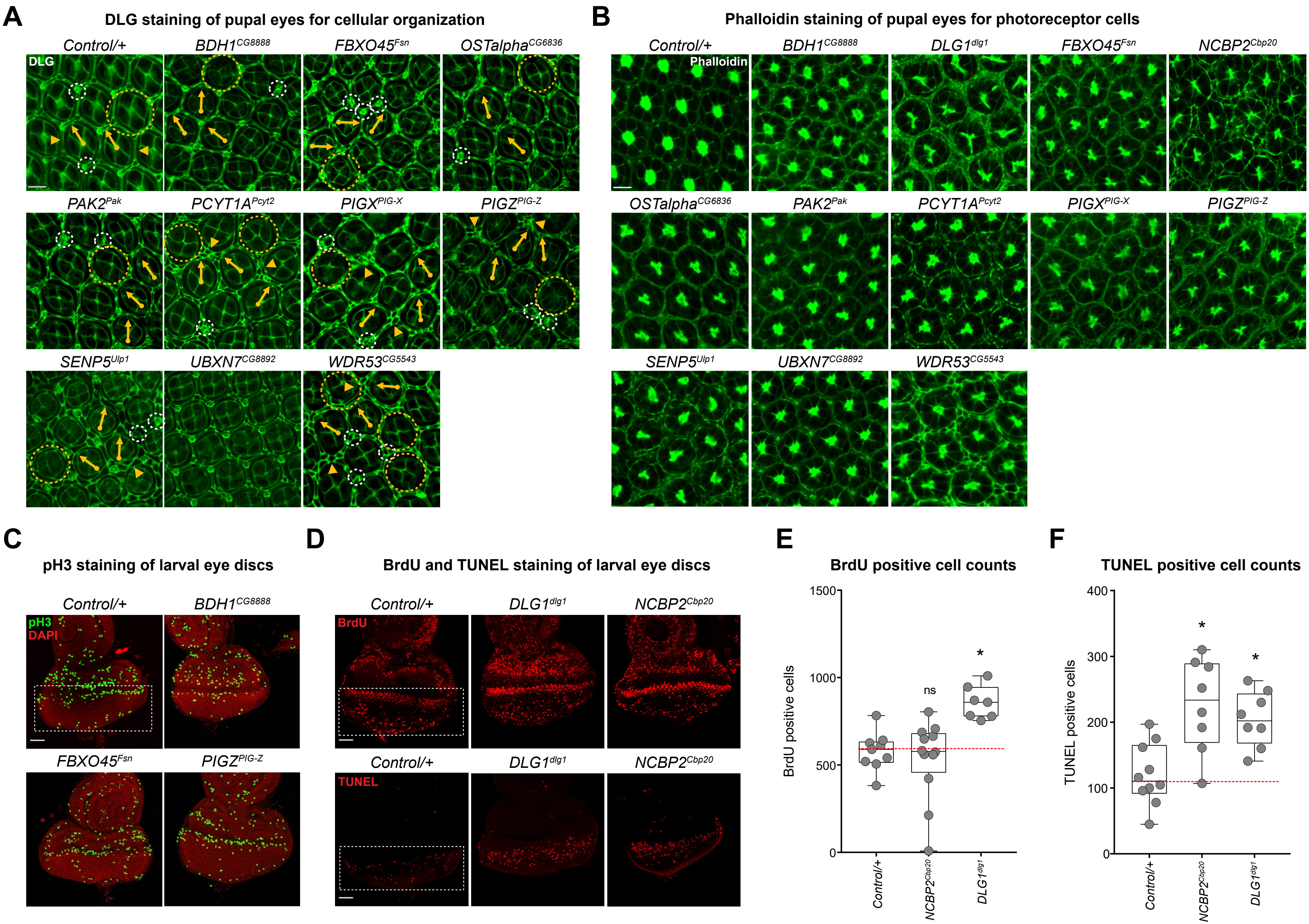

A
DLG staining of pupal eyes for cellular organization
Control/+
BDH1CG8888
FBXO45Fsn
OSTalphaCG6836
DLG
PAK2Pak
PCYT1APcyt2
PIGXPIG-X
PIGZPIG-Z
SENP5Ulp1
UBXN7CG8892
WDR53CG5543
B
Phalloidin staining of pupal eyes for photoreceptor cells
Control/+
BDH1CG8888
DLG1dlg1
FBXO45Fsn
NCBP2Cbp20
Phalloidin
OSTalphaCG6836
PAK2Pak
PCYT1APcyt2
PIGXPIG-X
PIGZPIG-Z
SENP5Ulp1
UBXN7CG8892
WDR53CG5543
C
pH3 staining of larval eye discs
Control/+
BDH1CG8888
pH3
DAPI
FBXO45Fsn
PIGZPIG-Z
D
BrdU and TUNEL staining of larval eye discs
Control/+
DLG1dlg1
NCBP2Cbp20
BrdU
TUNEL
E
BrdU positive cell counts
BrdU positive cells
1500
1000
500
0
ns
*
Control/+
NCBP2Cbp20
DLG1dlg1
F
TUNEL positive cell counts
TUNEL positive cells
400
300
200
100
0
*
*
Control/+
NCBP2Cbp20
DLG1dlg1

Figure S4. Cellular phenotypes of flies with eye-specific knockdown of individual 3q29 homologs. (A) Confocal images of pupal eyes (scale bar = 5 µm) stained with anti-DLG illustrate a range of defects in ommatidial organization upon knockdown of individual 3q29 homologs. Yellow circles indicate cone cell defects, white circles indicate bristle cell defects, yellow arrows indicate rotation defects, and yellow arrowheads indicate secondary cell defects. **(B)** Confocal images of pupal eyes (scale bar = 5 µm) stained with Phalloidin illustrate defects in photoreceptor cell count and organization upon knockdown of individual 3q29 homologs. (**C**) Confocal images of larval eye discs (scale bar = 30 µm) stained with anti-pH3 illustrate changes in cell proliferation upon knockdown of select individual 3q29 homologs. **(D)** Larval eye discs (scale bar = 30 µm) stained with BrdU (top) and TUNEL (bottom) illustrate abnormal cell cycle and apoptosis defects, respectively, due to eye-specific knockdown of $NCBP2^{Cbp20}$ and $DLG1^{dlg1}$. **(E)** Box plot of BrdU-positive cells in the larval eye discs of $DLG1^{dlg1}$ and $NCBP2^{Cbp20}$ flies (n = 7–12, *p < 0.05, two-tailed Mann–Whitney test). (**F**) Box plot of TUNEL-positive cells in the larval eye discs of $DLG1^{dlg1}$ and $NCBP2^{Cbp20}$ flies (n = 8, *p < 0.05, two-tailed Mann–Whitney test). All boxplots indicate median (center line), 25th and 75th percentiles (bounds of box), and minimum and maximum (whiskers).

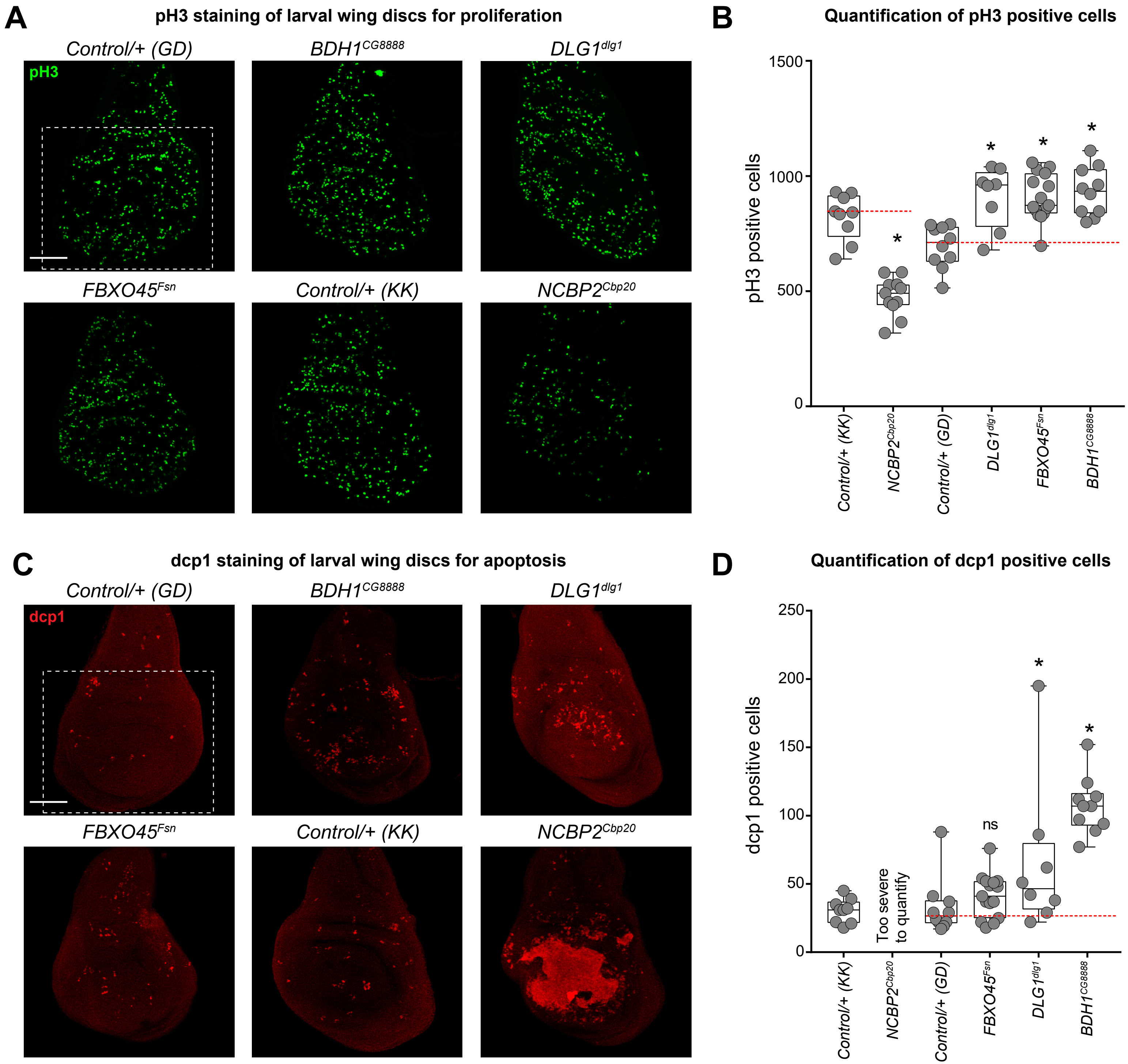
A
pH3 staining of larval wing discs for proliferation
Control/+ (GD)
BDH1 CG8888
DLG1 dlg1
pH3
FBXO45 Fsn
Control/+ (KK)
NCBP2 Cbp20
B
Quantification of pH3 positive cells
pH3 positive cells
1500
1000
500
0
*
Control/+ (KK)
NCBP2 Cbp20
Control/+ (GD)
DLG1 dlg1
FBXO45 Fsn
BDH1 CG8888
C
dcp1 staining of larval wing discs for apoptosis
Control/+ (GD)
BDH1 CG8888
DLG1 dlg1
dcp1
FBXO45 Fsn
Control/+ (KK)
NCBP2 Cbp20
D
Quantification of dcp1 positive cells
dcp1 positive cells
250
200
150
100
50
0
Too severe to quantify
ns
*
Control/+ (KK)
NCBP2 Cbp20
Control/+ (GD)
FBXO45 Fsn
DLG1 dlg1
BDH1 CG8888

Figure S5. Cellular phenotypes of flies with wing-specific knockdown of individual 3q29 homologs. (A) Larval wing discs (scale bar = 50 μm) stained with pH3 illustrate abnormal cell proliferation due to knockdown of select individual 3q29 homologs compared with appropriate VDRC GD and KK controls. We examined changes in the number of stained cells within the wing pouch of the wing disc (white box), which becomes the adult wing. **(B)** Box plot of pH3-positive cells in the larval wing discs of flies with knockdown of select 3q29 homologs (n = 8–15, *p < 0.05, two-tailed Mann–Whitney test). **(C)** Larval wing discs (scale bar = 50 μm) stained with anti-dcp1 show abnormal apoptosis due to knockdown of select individual 3q29 homologs compared with appropriate VDRC GD and KK controls. **(D)** Box plot of dcp1-positive cells in the larval wing discs of flies with knockdown of select individual 3q29 homologs (n = 8–15, *p < 0.05, two-tailed Mann–Whitney test). $NCBP2^{Cbp20}$ flies showed severe dcp1 staining across the entire wing disc and could not be quantified. All boxplots indicate median (center line), 25th and 75th percentiles (bounds of box), and minimum and maximum (whiskers).

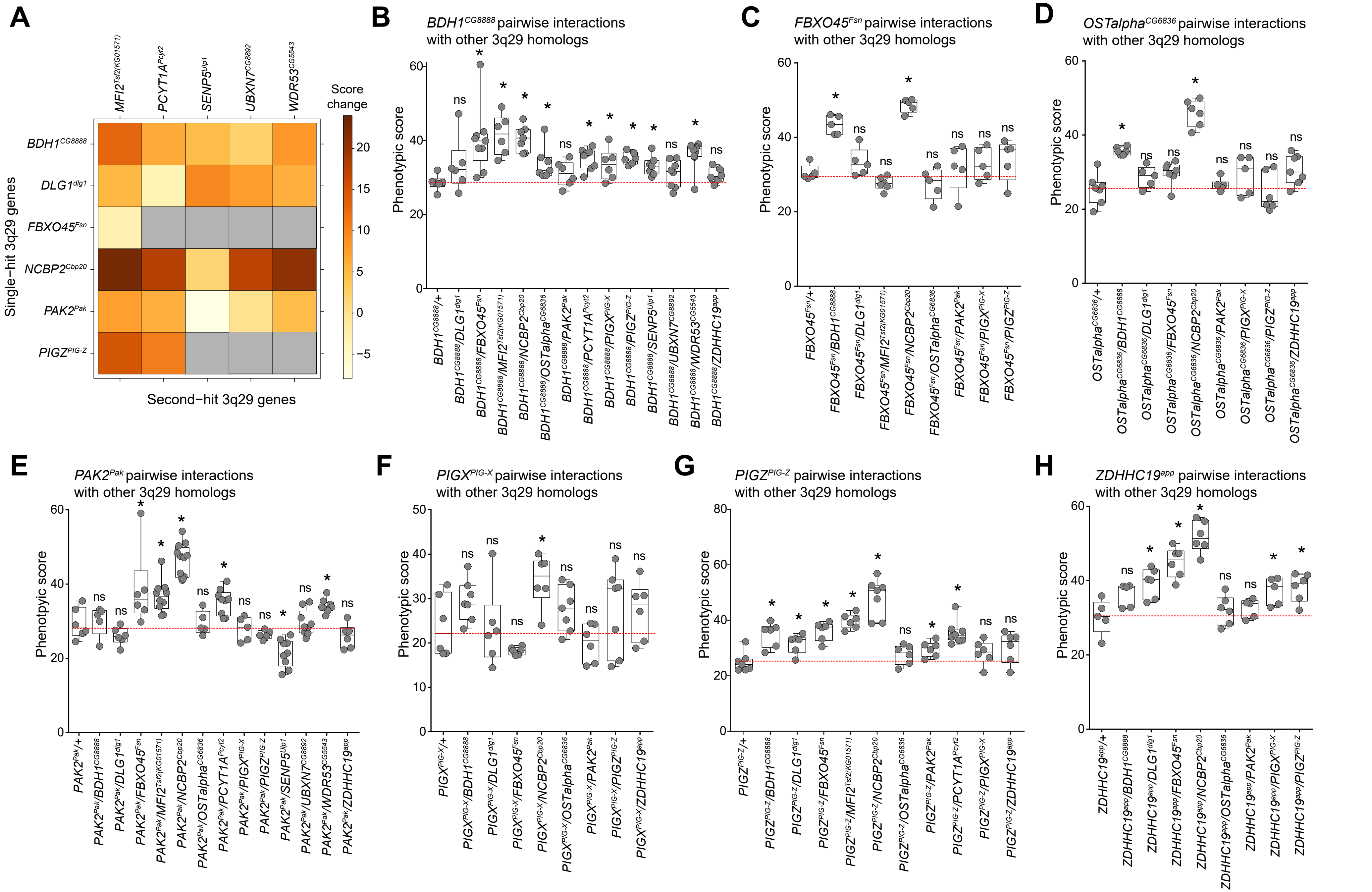
A
B
$BDH1^{CG8888}$ pairwise interactions with other 3q29 homologs
C
$FBXO45^{Fsn}$ pairwise interactions with other 3q29 homologs
D
$OSTalpha^{CG6836}$ pairwise interactions with other 3q29 homologs
E
$PAK2^{Pak}$ pairwise interactions with other 3q29 homologs
F
$PIGX^{PIG-X}$ pairwise interactions with other 3q29 homologs
G
$PIGZ^{PIG-Z}$ pairwise interactions with other 3q29 homologs
H
$ZDHHC19^{app}$ pairwise interactions with other 3q29 homologs
Score change
Single−hit 3q29 genes
Second−hit 3q29 genes
Phenotypic score
Phenotpyic score

Figure S6. Phenotypic screening for pairwise interactions of 3q29 homologs in the adult fly eye. (A) Heatmap showing average changes in phenotypic scores for pairwise interactions of 3q29 homologs in the adult eye, compared with single-hit recombined lines. Gray boxes indicate crosses without available data. Crosses with the mutant line *MFI2*$^{Tsf2(KG01571)}$ are included, as eye-specific RNAi knockdown of *MFI2*^{Tsf2} was lethal. **(B-H)** Box plots of phenotypic scores for pairwise knockdowns of 3q29 homologs compared with single-hit recombined lines ($n = 5–12$, $^*p < 0.05$, two-tailed Mann–Whitney test). All boxplots indicate median (center line), 25th and 75th percentiles (bounds of box), and minimum and maximum (whiskers).

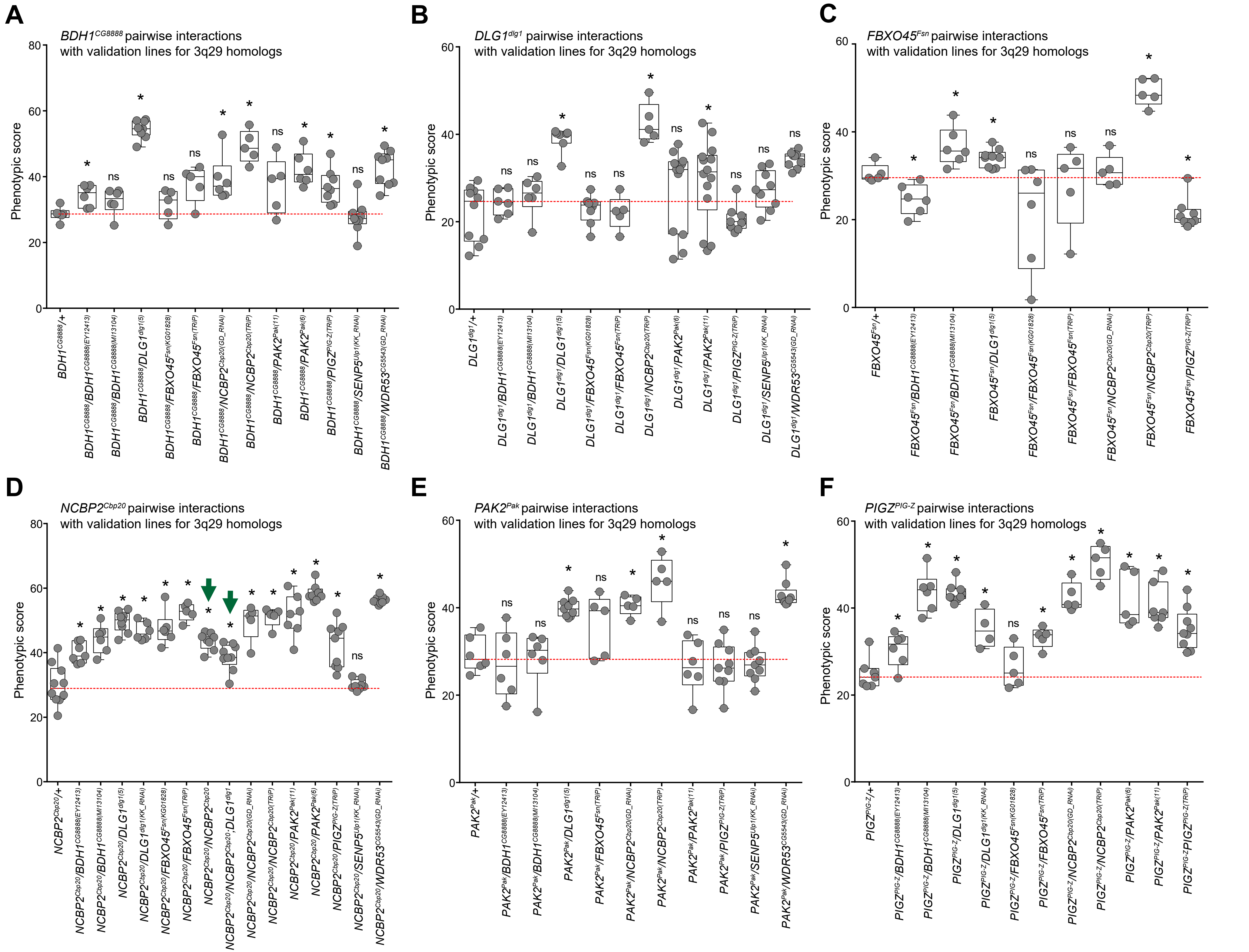

A
BDH1CG8888 pairwise interactions
with validation lines for 3q29 homologs
Phenotypic score
B
DLG1dlg1 pairwise interactions
with validation lines for 3q29 homologs
Phenotypic score
C
FBXO45Fsn pairwise interactions
with validation lines for 3q29 homologs
Phenotypic score
D
NCBP2Cbp20 pairwise interactions
with validation lines for 3q29 homologs
Phenotypic score
E
PAK2Pak pairwise interactions
with validation lines for 3q29 homologs
Phenotypic score
F
PIGZPIG-Z pairwise interactions
with validation lines for 3q29 homologs
Phenotypic score

Figure S7. Validation lines for pairwise interactions of 3q29 homologs in in the adult fly eye. (A-F) Box plots of phenotypic scores for pairwise knockdowns of select 3q29 homologs ($BDH1^{CG8888}$, $DLG1^{dlg1}$, $FBXO45^{Fsn}$, $NCBP2^{Cbp20}$, $PAK2^{Pak}$, and $PIGZ^{PIG\text{-}Z}$) with validation lines for other 3q29 homologs, compared with single-hit recombined lines ($n = 4$–14, *$p < 0.05$, two-tailed Mann–Whitney test). These crosses include homozygous $NCBP2^{Cbp20}/NCBP2^{Cbp20}$ knockdown and $DLG1^{dlg1}$ crossed with the homozygous $NCBP2^{Cbp20}$ knockdown (green arrows). All boxplots indicate median (center line), 25th and 75th percentiles (bounds of box), and minimum and maximum (whiskers).

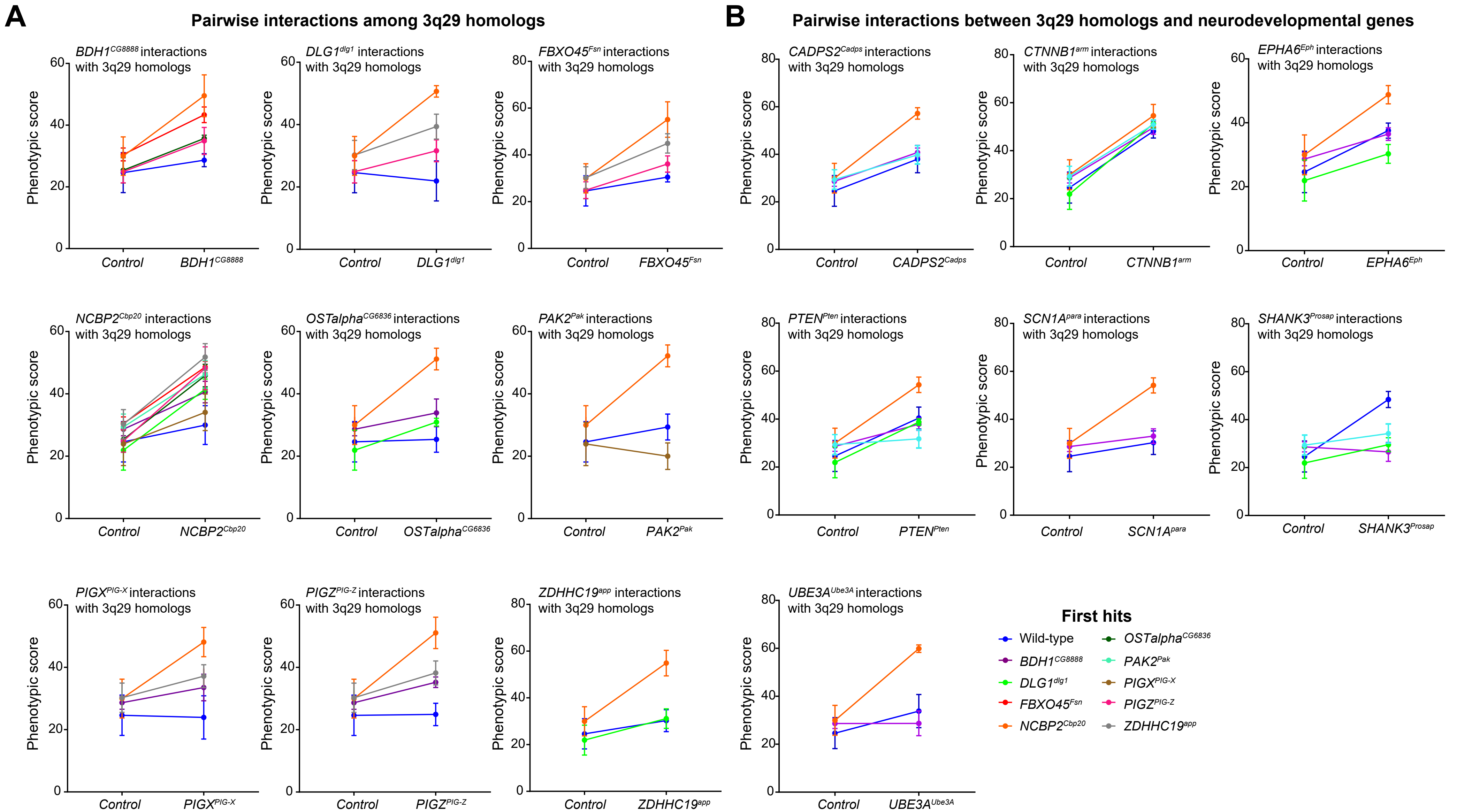

A
Pairwise interactions among 3q29 homologs
B
Pairwise interactions between 3q29 homologs and neurodevelopmental genes
BDH1CG8888 interactions with 3q29 homologs
DLG1dlg1 interactions with 3q29 homologs
FBXO45Fsn interactions with 3q29 homologs
CADPS2Cadps interactions with 3q29 homologs
CTNNB1arm interactions with 3q29 homologs
EPHA6Eph interactions with 3q29 homologs
NCBP2Cbp20 interactions with 3q29 homologs
OSTalphaCG6836 interactions with 3q29 homologs
PAK2Pak interactions with 3q29 homologs
PTENPten interactions with 3q29 homologs
SCN1Apara interactions with 3q29 homologs
SHANK3Prosap interactions with 3q29 homologs
PIGXPIG-X interactions with 3q29 homologs
PIGZPIG-Z interactions with 3q29 homologs
ZDHHC19app interactions with 3q29 homologs
UBE3AUbe3A interactions with 3q29 homologs
Phenotypic score
Control
First hits
Wild-type
BDH1CG8888
DLG1dlg1
FBXO45Fsn
NCBP2Cbp20
OSTalphaCG6836
PAK2Pak
PIGXPIG-X
PIGZPIG-Z
ZDHHC19app

Figure S8. Comparison of phenotypic scores for single-hit and two-hit knockdown of 3q29 homologs in the *Drosophila* eye. Phenotypic scores for **(A)** pairwise knockdowns between 3q29 homologs showing enhancement of the single-hit phenotypes and **(B)** pairwise knockdown of 3q29 homologs with other neurodevelopmental genes are compared with scores for single hits of both homologs and wild-type controls. Error bars indicate mean ± standard deviation of phenotypic scores for the selected genotypes (n=5–20). Phenotypic scores were compared using two-way ANOVA tests (see **Table S12**). Significant ANOVA results indicate pairwise interactions that suppress or synergistically enhance the respective single-hit phenotypes, while non-significant results indicate an additive interaction between the two genes.

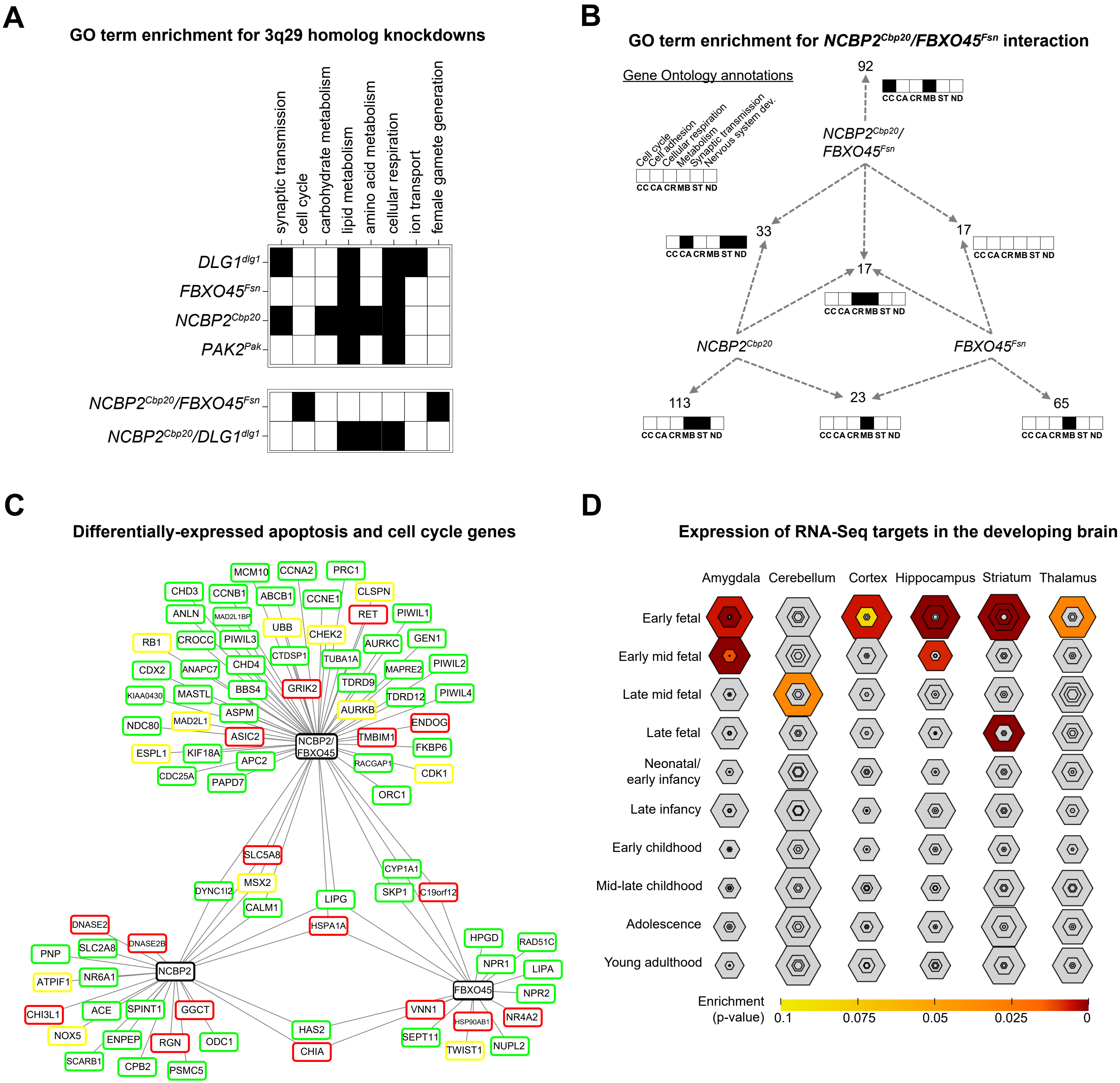

A
GO term enrichment for 3q29 homolog knockdowns
synaptic transmission
cell cycle
carbohydrate metabolism
lipid metabolism
amino acid metabolism
cellular respiration
ion transport
female gamete generation
DLG1dlg1
FBXO45Fsn
NCBP2Cbp20
PAK2Pak
NCBP2Cbp20/FBXO45Fsn
NCBP2Cbp20/DLG1dlg1
B
GO term enrichment for NCBP2Cbp20/FBXO45Fsn interaction
Gene Ontology annotations
Cell cycle
Cell adhesion
Cellular respiration
Metabolism
Synaptic transmission
Nervous system dev.
CC CA CR MB ST ND
92
NCBP2Cbp20/FBXO45Fsn
33
17
17
NCBP2Cbp20
FBXO45Fsn
113
23
65
C
Differentially-expressed apoptosis and cell cycle genes
MCM10
CCNA2
PRC1
CHD3
CCNB1
ABCB1
CCNE1
CLSPN
ANLN
MAD2L1BP
RET
PIWIL1
UBB
CHEK2
RB1
CROCC
PIWIL3
GEN1
CTDSP1
TUBA1A
AURKC
CDX2
ANAPC7
CHD4
PIWIL2
MAPRE2
KIAA0430
MASTL
BBS4
GRIK2
TDRD9
PIWIL4
TDRD12
ASPM
AURKB
NDC80
MAD2L1
ENDOG
ASIC2
NCBP2/FBXO45
TMBIM1
ESPL1
KIF18A
FKBP6
APC2
RACGAP1
CDC25A
PAPD7
CDK1
ORC1
SLC5A8
CYP1A1
MSX2
DYNC1I2
SKP1
C19orf12
LIPG
CALM1
DNASE2
HSPA1A
DNASE2B
HPGD
SLC2A8
RAD51C
PNP
NPR1
NCBP2
LIPA
NR6A1
ATPIF1
FBXO45
NPR2
CHI3L1
ACE
SPINT1
GGCT
VNN1
NR4A2
HSP90AB1
NOX5
ENPEP
HAS2
SEPT11
RGN
ODC1
TWIST1
NUPL2
SCARB1
CPB2
PSMC5
CHIA
D
Expression of RNA-Seq targets in the developing brain
Amygdala
Cerebellum
Cortex
Hippocampus
Striatum
Thalamus
Early fetal
Early mid fetal
Late mid fetal
Late fetal
Neonatal/early infancy
Late infancy
Early childhood
Mid-late childhood
Adolescence
Young adulthood
Enrichment (p-value)
0.1
0.075
0.05
0.025
0

Figure S9. Transcriptome analysis of flies with knockdown of select 3q29 homologs. (**A**) Clusters of Gene Ontology terms enriched among differentially expressed genes of 3q29 single and two-hit gene knockdowns ($p < 0.05$ with Benjamini-Hochsberg correction). Black boxes indicate enrichment of each gene set for clusters of Gene Ontology terms. Full lists of enriched GO terms are present in **Table S5**. (**B**) Enrichments for shared and unique differentially-expressed genes with individual knockdown of *NCBP2*^{Cbp20} and *FBXO45*^{Fsn} as well as concomitant knockdown of *NCBP2*^{Cbp20}/*FBXO45*^{Fsn}. Black boxes indicate enrichment of each gene set for clusters of Gene Ontology terms. We found 92 genes uniquely dysregulated in *NCBP2*^{Cbp20}/*FBXO45*^{Fsn} two-hit knockdown flies, which were enriched for cell cycle function. **(C)** Diagram showing differentially-expressed human cell cycle and apoptosis genes with knockdown of *NCBP2*^{Cbp20} and *FBXO45*^{Fsn}, as well as concomitant knockdown of *NCBP2*^{Cbp20}/*FBXO45*^{Fsn}. Red boxes indicate apoptosis genes, green boxes indicate cell cycle genes, and yellow boxes indicate genes associated with both functions. **(D)** Enrichment of human homologs of genes differentially expressed in *NCBP2*^{Cbp20}/*FBXO45*^{Fsn} knockdown flies across different brain tissues and developmental timepoints (Specific Expression Analysis). The size of each hexagon represents the number of genes preferentially expressed at each tissue and timepoint, with concentric hexagons representing bins of genes with stronger levels of preferential expression. The shading of each hexagon represents the enrichment of differentially-expressed genes among genes preferentially expressed at each timepoint ($p<0.1$, Fisher's Exact test with Benjamini-Hochberg correction).

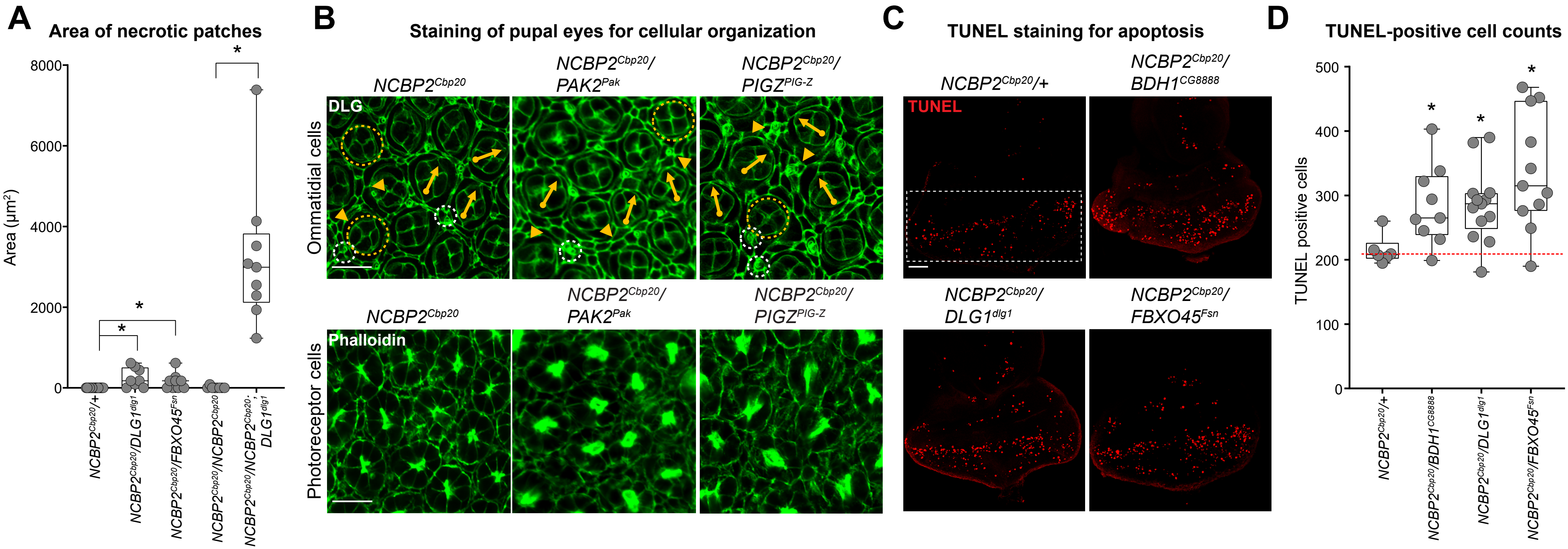
A
Area of necrotic patches
Area (µm²)
8000
6000
4000
2000
0
*
*
*
NCBP2Cbp20/+
NCBP2Cbp20/DLG1dlg1
NCBP2Cbp20/FBXO45Fsn
NCBP2Cbp20/NCBP2Cbp20
NCBP2Cbp20/NCBP2Cbp20; DLG1dlg1
B
Staining of pupal eyes for cellular organization
NCBP2Cbp20
NCBP2Cbp20/PAK2Pak
NCBP2Cbp20/PIGZPIG-Z
DLG
Ommatidial cells
Phalloidin
Photoreceptor cells
C
TUNEL staining for apoptosis
NCBP2Cbp20/+
NCBP2Cbp20/BDH1CG8888
TUNEL
NCBP2Cbp20/DLG1dlg1
NCBP2Cbp20/FBXO45Fsn
D
TUNEL-positive cell counts
TUNEL positive cells
500
400
300
200
100
0
*
*
*
NCBP2Cbp20/+
NCBP2Cbp20/BDH1CG8888
NCBP2Cbp20/DLG1dlg1
NCBP2Cbp20/FBXO45Fsn

Figure S10. Cellular phenotypes for pairwise knockdowns of 3q29 homologs. (**A**) Box plot showing area of necrotic patches in adult fly eyes with knockdown of *FBXO45*^{Fsn} or *DLG1*^{dlg1} and heterozygous or homozygous knockdown of *NCBP2*^{Cbp20} (n=8-9, *p < 0.05, two-tailed Mann–Whitney test). **(B)** Confocal images of pupal eyes (scale bar = 5 µm) stained with DLG (top) and Phalloidin (bottom) illustrate enhanced defects in ommatidial and photoreceptor cell organization with concomitant knockdown of *NCBP2*^{Cbp20} and other 3q29 homologs compared with *NCBP2*^{Cbp20} knockdown. (**C**) Larval eye discs (scale bar = 30 µm) stained with TUNEL show increases in apoptosis with pairwise knockdown of *NCBP2*^{Cbp20} and other 3q29 homologs compared with *NCBP2*^{Cbp20} knockdown. (**D**) Box plot of TUNEL-positive cells in the larval eye discs of 3q29 two-hit knockdown flies (n = 9–13, *p < 0.05, two-tailed Mann–Whitney test). All boxplots indicate median (center line), 25th and 75th percentiles (bounds of box), and minimum and maximum (whiskers).

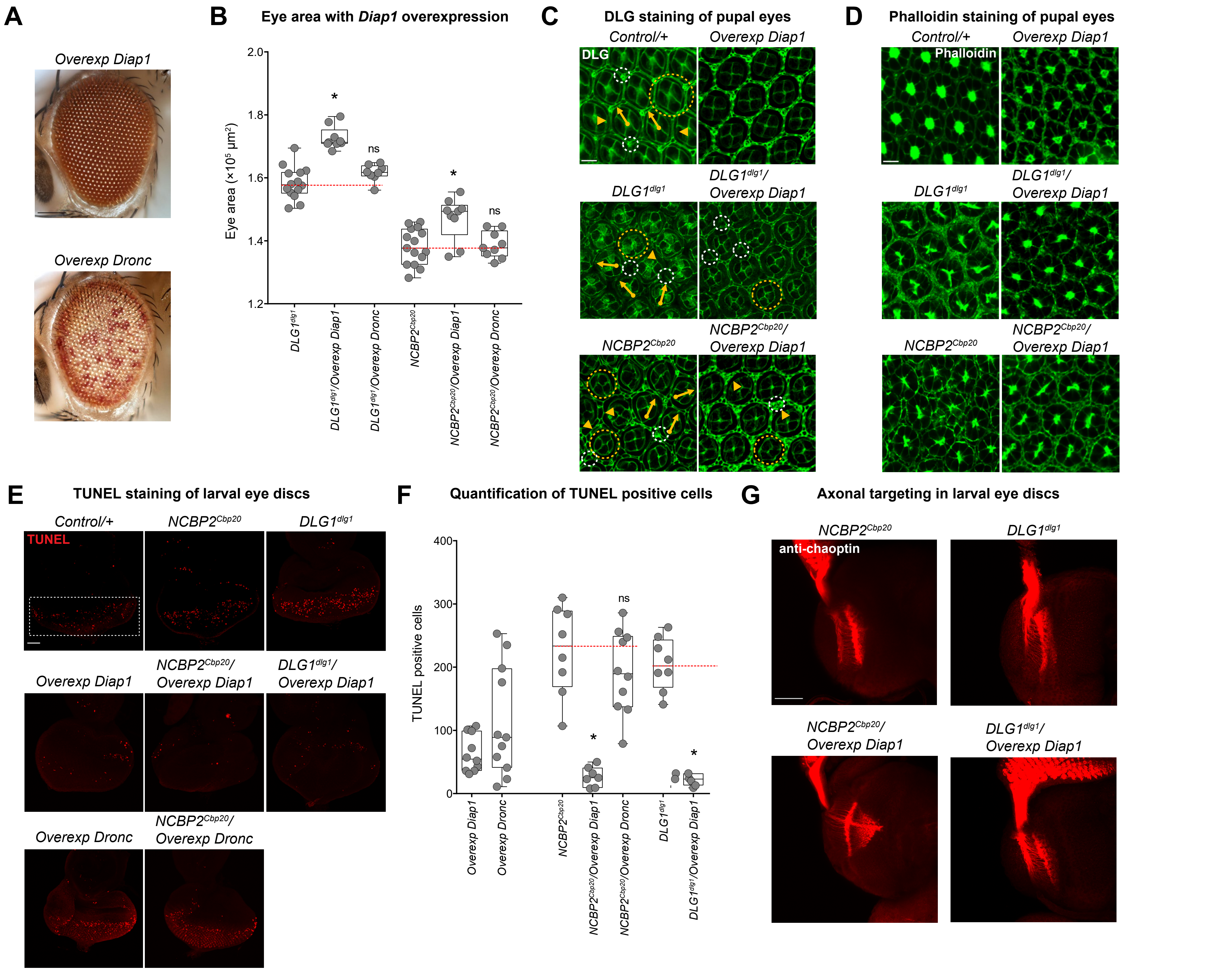

A
Overexp Diap1
Overexp Dronc
B
Eye area with Diap1 overexpression
Eye area (×10^5 μm^2)
2.0
1.8
1.6
1.4
1.2
*
ns
*
ns
DLG1^{dlg1}
DLG1^{dlg1}/Overexp Diap1
DLG1^{dlg1}/Overexp Dronc
NCBP2^{Cbp20}
NCBP2^{Cbp20}/Overexp Diap1
NCBP2^{Cbp20}/Overexp Dronc
C
DLG staining of pupal eyes
Control/+
Overexp Diap1
DLG
DLG1^{dlg1}
DLG1^{dlg1}/ Overexp Diap1
NCBP2^{Cbp20}
NCBP2^{Cbp20}/ Overexp Diap1
D
Phalloidin staining of pupal eyes
Control/+
Overexp Diap1
Phalloidin
DLG1^{dlg1}
DLG1^{dlg1}/ Overexp Diap1
NCBP2^{Cbp20}
NCBP2^{Cbp20}/ Overexp Diap1
E
TUNEL staining of larval eye discs
Control/+
NCBP2^{Cbp20}
DLG1^{dlg1}
TUNEL
Overexp Diap1
NCBP2^{Cbp20}/ Overexp Diap1
DLG1^{dlg1}/ Overexp Diap1
Overexp Dronc
NCBP2^{Cbp20}/ Overexp Dronc
F
Quantification of TUNEL positive cells
TUNEL positive cells
400
300
200
100
0
ns
*
*
Overexp Diap1
Overexp Dronc
NCBP2^{Cbp20}
NCBP2^{Cbp20}/Overexp Diap1
NCBP2^{Cbp20}/Overexp Dronc
DLG1^{dlg1}
DLG1^{dlg1}/Overexp Diap1
G
Axonal targeting in larval eye discs
NCBP2^{Cbp20}
DLG1^{dlg1}
anti-chaoptin
NCBP2^{Cbp20}/ Overexp Diap1
DLG1^{dlg1}/ Overexp Diap1

Figure S11. Rescue of cellular phenotypes of 3q29 knockdown flies with overexpression of *Diap1*. (A) Representative brightfield adult eye images of flies with overexpression of *Diap1* and *Dronc* (scale bar = 100 µm). (**B**) Box plot of adult eye area in 3q29 single-hit knockdown flies with *Diap1* and *Dronc* overexpression (n = 8–9, $*p < 0.05$, two-tailed Mann–Whitney test). **(C)** Confocal images of pupal eyes (scale bar = 5 µm) stained with anti-DLG illustrate the rescue of ommatidial organization defects due to knockdown of 3q29 homologs upon overexpression of *Diap1*. **(D)** Confocal images of pupal eyes (scale bar = 5 µm) stained with Phalloidin illustrate the rescue of photoreceptor cell organization defects due to knockdown of 3q29 homologs upon overexpression of *Diap1*. **(E)** Larval eye discs (scale bar = 30 µm) stained with TUNEL show rescue of apoptosis phenotypes observed in flies with knockdown of 3q29 homologs and overexpression of *Diap1*, as well as enhanced apoptosis with overexpression of *Dronc*. (**F**) Box plot of TUNEL-positive cells in the larval eye discs of 3q29 single-hit knockdown flies with overexpression of *Diap1* and *Dronc* (n = 7–10, $*p < 0.05$, two-tailed Mann–Whitney test). **(G)** Representative confocal images of larval eye discs stained with anti-chaoptin (scale bar = 30 µm) illustrate the rescue of axonal targeting defects observed in flies due to knockdown of 3q29 homologs with overexpression of *Diap1*. All boxplots indicate median (center line), 25th and 75th percentiles (bounds of box), and minimum and maximum (whiskers).

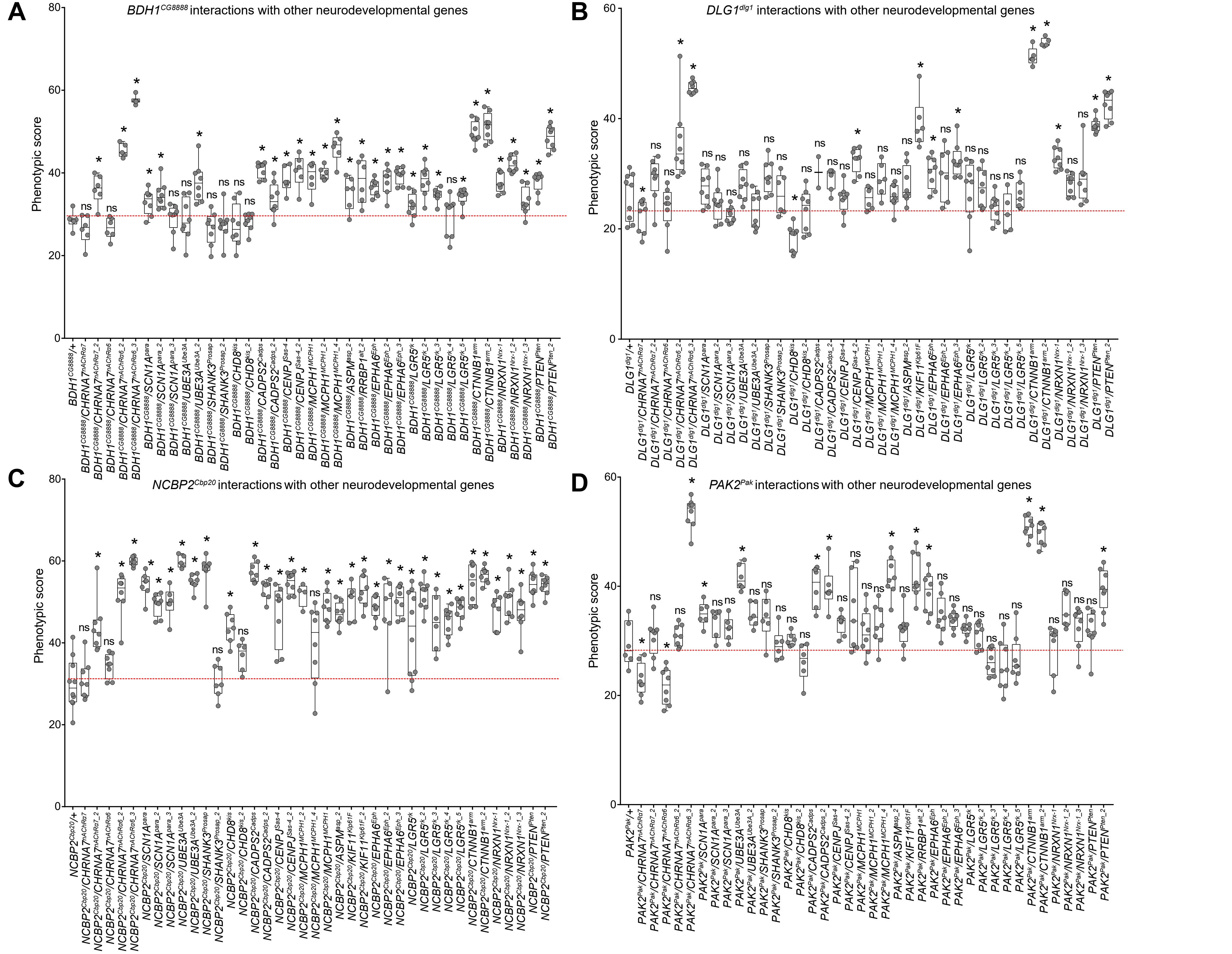

A
BDH1^CG8888 interactions with other neurodevelopmental genes
Phenotypic score
B
DLG1^dlg1 interactions with other neurodevelopmental genes
Phenotypic score
C
NCBP2^Cbp20 interactions with other neurodevelopmental genes
Phenotypic score
D
PAK2^Pak interactions with other neurodevelopmental genes
Phenotypic score

Figure S12. Phenotypic scores for interactions between 3q29 homologs and other neurodevelopmental genes in the adult fly eye. (A-D) Box plots of phenotypic scores for simultaneous knockdowns of 3q29 homologs and other neurodevelopmental genes compared with single-hit recombined lines ($n = 2–10$, $*p < 0.05$, two-tailed Mann–Whitney test). All boxplots indicate median (center line), 25th and 75th percentiles (bounds of box), and minimum and maximum (whiskers).

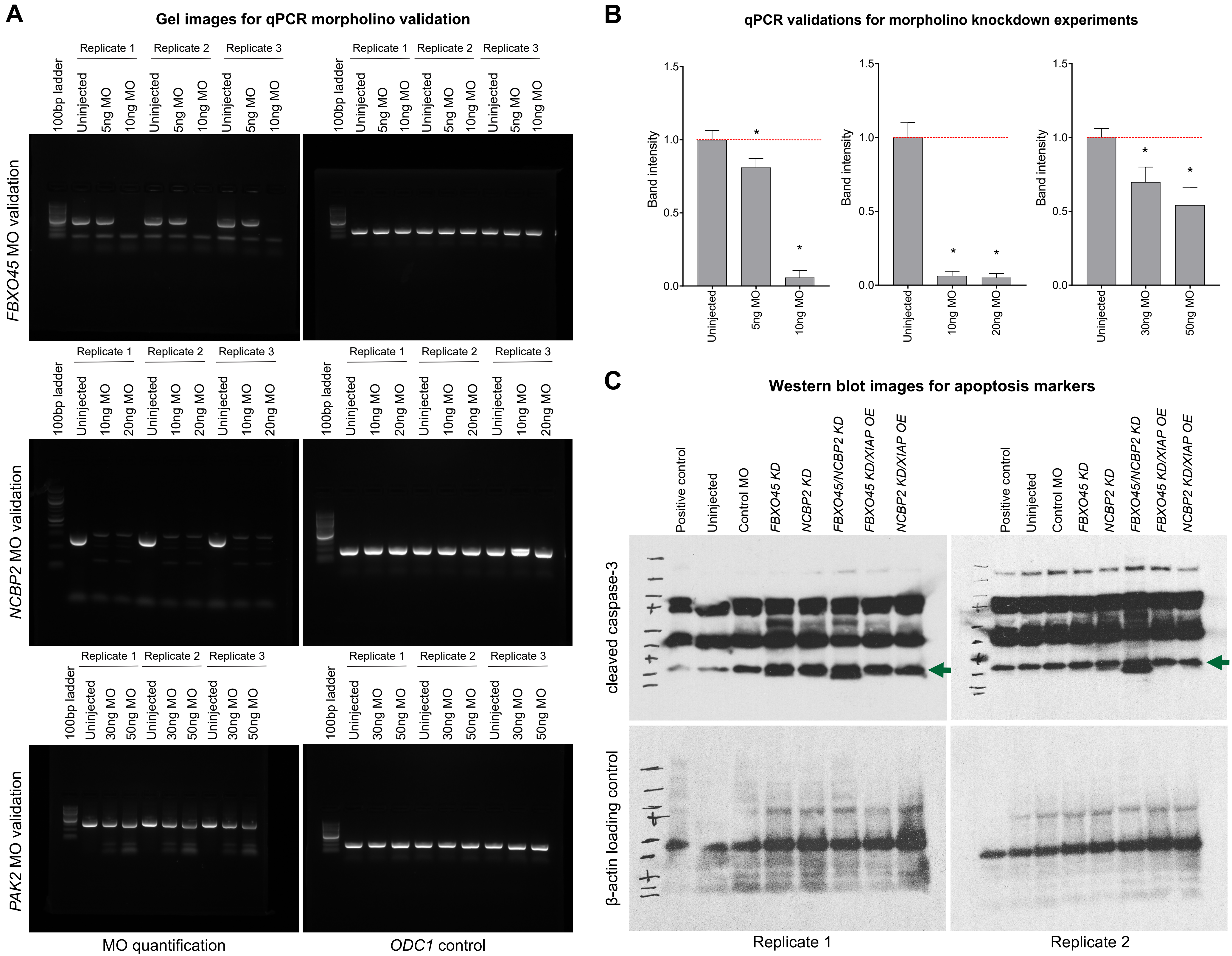
A
Gel images for qPCR morpholino validation
Replicate 1
Replicate 2
Replicate 3
100bp ladder
Uninjected
5ng MO
10ng MO
FBXO45 MO validation
20ng MO
NCBP2 MO validation
30ng MO
50ng MO
PAK2 MO validation
MO quantification
ODC1 control
B
qPCR validations for morpholino knockdown experiments
Band intensity
1.5
1.0
0.5
0.0
*
C
Western blot images for apoptosis markers
Positive control
Control MO
FBXO45 KD
NCBP2 KD
FBXO45/NCBP2 KD
FBXO45 KD/XIAP OE
NCBP2 KD/XIAP OE
cleaved caspase-3
β-actin loading control
Replicate 1
Replicate 2

Figure S13. Quantification of 3q29 morpholino knockdown and apoptosis marker levels in *X. laevis* models. (A) Electrophoretic gels show decreased expression of 3q29 genes due to morpholino (MO) knockdown at various concentrations in *X. laevis* embryos. Three replicates (uninjected and two MO concentrations) were performed for each morpholino, and band intensities were compared with expression of *ODC1* controls taken from the same cDNA samples and run on gels processed in parallel. **(B)** Quantification of 3q29 homolog expression at different MO concentrations, as measured by band intensity ratio to *ODC1* controls (n=3 replicates, *$p<0.05$, two-tailed Welch's T-test). **(C)** Full images of Western blots for quantification of cleaved caspase-3 levels in *X. laevis* embryos with MO knockdown of 3q29 homologs. Two replicate experiments were performed, and the intensity of bands at 19kD and 17kD (green arrows), corresponding with caspase-3, were normalized to those for the β-actin loading controls. Embryos injected with control MO, uninjected embryos, and embroys treated with 30% EtOH as a positive control were included with the embryos injected with 3q29 MOs.

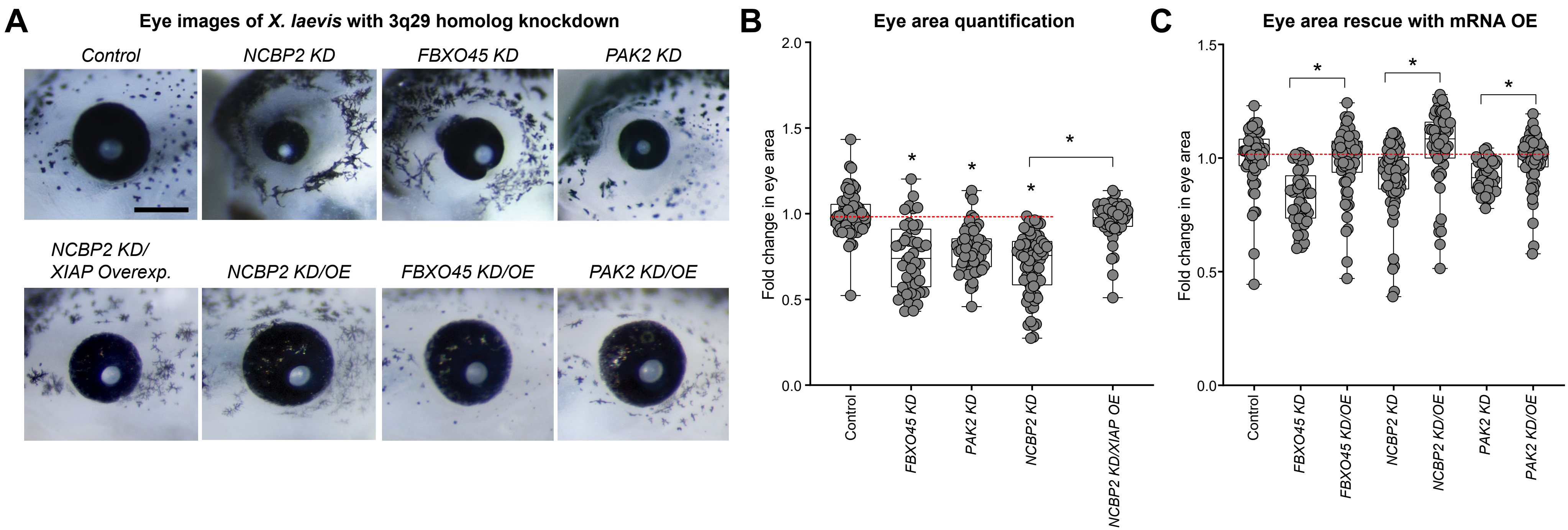
A
Eye images of X. laevis with 3q29 homolog knockdown
Control
NCBP2 KD
FBXO45 KD
PAK2 KD
NCBP2 KD/
XIAP Overexp.
NCBP2 KD/OE
FBXO45 KD/OE
PAK2 KD/OE
B
Eye area quantification
Fold change in eye area
2.0
1.5
1.0
0.5
0.0
Control
FBXO45 KD
PAK2 KD
NCBP2 KD
NCBP2 KD/XIAP OE
C
Eye area rescue with mRNA OE
Fold change in eye area
1.5
1.0
0.5
0.0
Control
FBXO45 KD
FBXO45 KD/OE
NCBP2 KD
NCBP2 KD/OE
PAK2 KD
PAK2 KD/OE

Figure S14. Eye phenotypes observed with knockdown of 3q29 homologs in *X. laevis* models. (A) Representative eye images of stage 42 *X. laevis* tadpoles with MO knockdown of 3q29 homologs (scale bar = 500 µm) show defects in eye size and morphology compared with the control (top). These defects were rescued with co-injection and overexpression of 3q29 homolog mRNA, as well as overexpression of the apoptosis inhibitor *XIAP1* for *NCBP2* (bottom). (**B**) Box plot of eye area in *X. laevis* models with knockdown of 3q29 homologs, normalized to controls (n = 48–71, *p < 0.05, two-tailed Welch's T-test). Models with *NCBP2* knockdown and *XIAP1* overexpression showed an increased eye size compared with *NCBP2* knockdown. (C) Box plot of eye area in *X. laevis* models with knockdown of 3q29 homologs and overexpression of 3q29 homolog mRNA, normalized to controls (n = 56–63, *p < 0.05, two-tailed Welch's T-test).

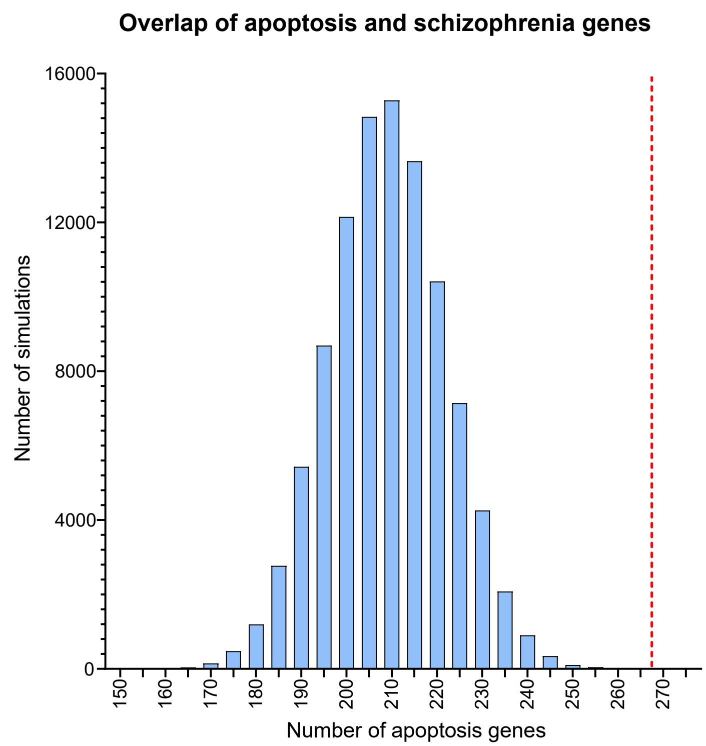
Overlap of apoptosis and schizophrenia genes
Number of simulations
Number of apoptosis genes
16000
12000
8000
4000
0
150
160
170
180
190
200
210
220
230
240
250
260
270

Figure S15. Simulation of schizophrenia-apoptosis gene overlap. We randomly selected 100,000 sets of 2,546 genes each and determined the number of genes in each set that were annotated for apoptosis-related GO terms. The red dotted line indicates the number of apoptosis genes (268) observed in our set of 2,546 schizophrenia genes, which is in the top 98.64% of the simulation results. Candidate schizophrenia genes involved in apoptotic processes are listed in **Table S9**.

Supplementary Tables

Table S1. *Drosophila* homologs of human 3q29 genes and expression of *Drosophila* homologs during development.

Human gene	**Fly homolog**	**Identity (%)**	**Similarity (%)**	**DIOPT score**	**DIOPT rank**	**Larval central nervous system expression** (FlyAtlas)	**Larval eye expression** (modENCODE)
BDH1	*CG8888*	33	53	9	High	Low	NA
DLG1	*dlg1*	44	58	13	High	Moderate	Moderate
FBXO45	*Fsn*	71	84	13	High	Moderate	Moderate
MFI2	*Tsf2*	33	48	15	High	Low	Moderate
NCBP2	*Cbp20*	78	89	14	High	Moderate	Moderate
OSTalpha	*CG6836*	19	40	5	High	Low	Low
PAK2	*Pak*	42	50	10	Moderate	NA	Moderate
PCYT1A	*Pcyt2*	58	72	12	High	Moderate	Moderate
PIGX	*PIG-X*	24	39	7	High	Low	Low
PIGZ	*PIG-Z*	30	41	10	High	NA	Low
SENP5	*Ulp1*	21	35	2	Low	Moderate	Low
TCTEX1D2	*CG5359*	33	51	9	Moderate	Moderate	Low
UBXN7	*CG8892*	28	43	13	High	Moderate	Moderate
WDR53	*CG5543*	21	34	NA	NA	Low	Moderate
ZDHHC19	*app*	34	49	3	Moderate	NA	Low
CEP19	None						
LRRC33	None						
RNF68	None						
SMCO1	None						
TFRC	None						
TM4SF19	None						

DIOPT version 7.1 (3) and reciprocal BLAST was used to identify fly homologs of 3q29 genes; six genes did not have fly homologs. Expression levels of fly homologs of 3q29 genes were assessed using high-throughput expression data from FlyAtlas Anatomy microarray expression data (4) and modENCODE Anatomy RNA-Seq data (5) from www.flybase.com.

Table S2. qPCR primers and expression values for RNAi knockdown of 3q29 homologs.

Gene name	Forward and reverse primers	Expression (%)	SE (%)	p-value	*tiptop* expression (%)
BDH1^{CG8888}	For-5'- TTCGCAAGAGCTTGGACCTC-3' Rev-5'- TTTGTGTTAGCCGAGCGGAA-3'	25.005	4.514	0.016	--
DLG1^{dlg1}	For-5'- ACACAAGACGATGCCAATGC-3' Rev-5'- TCCACCCTGTAGATAATCTCGC-3'	62.691	5.935	0.014	--
FBXO45^{Fsn}	For-5'- CCCATTTGGTTGGTGTGGGA-3' Rev-5'- TGGATTTACCCGTTCCTGTTGA-3'	55.230	13.387	0.017	--
NCBP2^{Cbp20}	For-5'- TTGTGAATGGCACTCGCTTG-3' Rev-5'- GTCCCAGTCCACACGAATCA-3'	43.900	7.815	0.006	67.213
OSTalpha^{CG6836}	For-5'- CCCTTCATCGTCTGCTCCAT-3' Rev-5'- GTGATTTGGAGGGACCAAGC-3'	49.087	10.141	0.090	52.470
PAK2^{Pak}	For-5'- GTCGTCACCCGGAAACAGTA-3' Rev-5'- GCCCAAAGACCAAAGGTCCA-3'	40.212	5.100	0.002	45.966
PCYT1A^{Pcyt2}	For-5'- CGCTACGTGGATGAGATCGT-3' Rev-5'- TCCTCATTTAGCGTCCACGG-3'	80.642	3.377	0.022	--
PIGX$^{PIG\text{-}X}$	For-5'- TGACCTGCAGCGTTTGAAGA-3' Rev-5'- TGACGAACTTAGGATAGATGGCA-3'	29.775	7.899	0.023	36.777
PIGZ$^{PIG\text{-}Z}$	For-5'-TCCAGAGCGTGGAGGTAATG-3' Rev-5'- CGTATGCTCCAGCCGAAAGT-3'	37.856	3.355	0.045	45.199
SENP5^{Ulp1}	For-5'-CCTGGCCAAGGGCTAAAAGT-3' Rev-5'- GACATGCGTGTGTTCGCTAC-3'	30.077	4.202	1.51E-4	--
TCTEX1D2^{CG5359}	For-5'- ACGTTATGGCCGAGAAACTCA-3' Rev-5'-TGGCGACGTCCTTGTCATAG-3'	20.945	8.807	0.113	152.953
UBXN7^{CG8892}	For-5'- TCCAGAGCAACGTCATGTCC-3' Rev-5'- TGGACCGTCTGTTAAGTGCC-3'	45.885	8.430	0.018	--
WDR53^{CG5543}	For-5'- AAATCCACTTAGCGTGGGGC-3' Rev-5'- AGGAAATTTTACCGCGTTGCAT-3'	49.764	1.756	0.005	--
ZDHHC19^{app}	For-5'- GCGATCAGACAACCAACGAG-3' Rev-5'- CGCCTTTGGAGGAGAAGGAT-3'	56.304	14.891	0.050	39.256
Rp49 control	For-5'-GCAAGCCCAAGGGTATCGA-3' Rev-5'-ACCGATGTTGGGCATCAGA-3'	--	--	--	--
tiptop	For-5'-CCTCCACAGCATCAGCAACA-3' Rev-5'-CCACCAGGTCGTTACCGTTC-3'	--	--	--	--

Elav-GAL4 flies were crossed with RNAi lines of 3q29 fly homologs at 25°C, and 3-4 day old adult *Drosophila* heads were used to quantify the level of expression compared with controls. *TCTEX1D2*^{CG5359} flies did not show decreased expression (p>0.1) and also showed increased *tiptop* expression (6), and were therefore excluded from further experiments.

Table S3. Analysis of defects in ommatidial cells with knockdown of 3q29 homologs.

Gene	Cone cell defects	Primary cell defect	Secondary cell defect	Bristle group defect	Rotation error	Hexagonal defect	Photoreceptor defect
Control/+							
BDH1^{CG8888}	++			+	++		++
DLG1^{dlg1}	++		+	+++	+	++	+++
FBXO45^{Fsn}	++	+		++	++	+	
NCBP2^{Cbp20}	++	+	++	++	++	++	+++
OSTalpha^{CG6836}	+			+	+		+
PAK2^{Pak}	+			+	+	+	
PCYT1A^{Pcyt2}	+	++	++	++	++	+	+
PIGX$^{PIG\text{-}X}$	+		+	++	++		+
PIGZ$^{PIG\text{-}Z}$	+		+	++	+	+	++
SENP5^{Ulp1}	+	++	++	+	++	+	+
UBXN7^{CG8892}							+
WDR53^{CG5543}	++	++	++	+++	++	+	+

The number of "+" symbols indicate the severity of the observed cellular defects.

Table S4. Screening for pairwise interactions among 3q29 homologs.

Second-hit gene	*BDH1*^{CG8888}	*DLG1*^{dlg1}	*FBXO45*^{Fsn}	*NCBP2*^{Cbp20}	*OSTalpha*^{CG6836}	*PAK2*^{Pak}	*PIGX*$^{PIG\text{-}X}$	*PIGZ*$^{PIG\text{-}Z}$	*ZDHHC19*^{app}
BDH1^{CG8888}	Not validated (1/2)	Not validated (1/3)	Enhancer** (2/3)	Enhancer** (3/3)	Enhancer* (1/1)	No interaction (0/3)	No interaction (0/1)	Enhancer* (3/3)	No interaction (0/1)
DLG1^{dlg1}	Not validated (1/2)	Enhancer (1/1)	Not validated (1/2)	Enhancer** (4/4)	No interaction (0/1)	Not validated (1/2)	No interaction (0/1)	Enhancer** (3/3)	Enhancer** (1/1)
FBXO45^{Fsn}	Not validated (1/3)	Not validated (1/3)	No interaction (0/2)	Enhancer** (3/3)	No interaction (0/1)	Not validated (1/2)	No interaction (0/1)	Enhancer* (2/3)	Enhancer** (1/1)
NCBP2^{Cbp20}	Enhancer* (3/3)	Enhancer** (2/2)	Enhancer** (2/3)	Enhancer (3/3)	Enhancer** (1/1)	Enhancer** (3/3)	Enhancer* (1/1)	Enhancer** (3/3)	Enhancer** (1/1)
OSTalpha^{CG6836}	Enhancer* (1/1)	Enhancer** (1/1)	No interaction (0/1)	Enhancer** (1/1)	NA	No interaction (0/1)	No interaction (0/1)	No interaction (0/1)	No interaction (0/1)
PAK2^{Pak}	Not validated (1/3)	Not validated (1/3)	No interaction (0/3)	Enhancer** (3/3)	No interaction (0/1)	No interaction (0/1)	No interaction (0/1)	Enhancer* (3/3)	No interaction (0/1)
PIGX$^{PIG\text{-}X}$	Enhancer* (1/1)	No interaction (0/1)	No interaction (0/1)	Enhancer** (1/1)	No interaction (0/1)	No interaction (0/1)	NA	No interaction (0/1)	Enhancer* (1/1)
PIGZ$^{PIG\text{-}Z}$	Enhancer* (2/2)	Not validated (1/2)	Not validated (1/2)	Enhancer** (2/2)	No interaction (0/1)	No interaction (0/2)	No interaction (0/1)	Enhancer (1/1)	Enhancer* (1/1)
ZDHHC19^{app}	No interaction (0/1)	Enhancer* (1/1)	NA	Enhancer** (1/1)	No interaction (0/1)	No interaction (0/1)	No interaction (0/1)	No interaction (0/1)	NA
MFI2$^{Tsf2(KG01571)}$	Enhancer (1/1)	No interaction (0/1)	No interaction (0/1)	Enhancer (1/1)	NA	Enhancer (1/1)	NA	Enhancer (1/1)	NA
PCYT1A^{Pcyt2}	Enhancer (1/1)	No interaction (0/1)	NA	Enhancer (1/1)	NA	Enhancer (1/1)	NA	Enhancer (1/1)	NA
SENP5^{Ulp1}	Not validated (1/2)	Not validated (1/2)	NA	No interaction (0/2)	NA	Not validated (1/2)	NA	NA	NA
UBXN7^{CG8892}	No interaction (0/1)	Enhancer (1/1)	NA	Enhancer (1/1)	NA	No interaction (0/1)	NA	NA	NA
WDR53^{CG5543}	Enhancer (2/2)	Not validated (1/2)	NA	Enhancer (2/2)	NA	Enhancer (2/2)	NA	NA	NA
Lines tested **(163 total)**	25	24	18	28	8	23	8	21	8
All interactions **(59/94 total)**	11/13	10/13	4/8	12/13	2/8	7/13	1/8	7/10	5/8
Validated **(44/94 total)**	7/13	4/13	2/8	12/13	2/8	4/13	1/8	7/10	5/8
Reciprocal cross **(21/30 total)**	3/4	1/3	1/2	8/8	2/2	1/1	1/1	2/5	2/4
Synergistic int. **(19/31 total)**	0/4	2/3	2/2	8/8	1/2	1/1	0/1	2/5	3/5

“All interactions” indicates the number of crosses where any single two-hit line showed enhancement of the single-hit phenotype, while “Validated” indicates the number of interactions which have at least an additional cross with a second line (if available) that confirmed the same result. “Reciprocal cross” indicates the number of interactions with concordant results across pairs of reciprocal cross (i.e. *NCBP2*^{Cbp20}/*DLG1*^{dlg1} vs. *DLG1*^{dlg1}/*NCBP2*^{Cbp20}). “Synergistic int.” indicates the number of enhancer interactions that are due to synergistic effects (**) compared with those due to additive effects (*), as determined by two-way ANOVA tests (**Supp. Figure 7**). These totals include crosses with the mutant line *MFI2*$^{Tsf2(KG01571)}$, as eye-specific RNAi knockdown of *MFI2*^{Tsf2} was lethal, as well as *DLG1*^{dlg1} crossed with homozygous *NCBP2*^{Cbp20}/*NCBP2*^{Cbp20} knockdown. Crosses with other lines for the same gene (shaded in grey) are included as validation lines tested but were not counted as interactions.

Table S5. Transcriptome analysis of 3q29 knockdown flies (Excel file). This file lists all differentially expressed genes from RNA sequencing of 3q29 knockdown flies with log-fold change >1 or < -1 and false discovery rate (FDR) <0.05. Human homologs identified using DIOPT are included for each differentially-expressed gene. The file also includes enriched Gene Ontology (GO) terms (p<0.05 with Benjamini-Hochsberg correction) for each set of differentially-expressed genes.

Table S6. Analysis of defects in ommatidial cells with pairwise knockdown of 3q29 homologs.

Pairwise cross	Cone cell defects			Primary cell defect	Secondary cell defect	Bristle cell defect	Rotation error	Hexagonal defect	Photoreceptor defect
	Number error	Arrangement error	Orientation error						
DLG1^{dlg1}			++		+	+++	+	++	+++
NCBP2^{Cbp20}			++	+	++	++	++	++	+++
NCBP2^{Cbp20}/ *BDH1*^{CG8888}	+	++	++	++	++	++	++	+++	++++
NCBP2^{Cbp20}/ *DLG1*^{dlg1}	+	++	++	++	++	+++	++	+	++++
NCBP2^{Cbp20}/ *FBXO45*^{Fsn}	+	++	++	++	+++	+++	++	++++	++++
NCBP2^{Cbp20}/ *PAK2*^{Pak}		++	++	+	++	++	+	+	+++
NCBP2^{Cbp20}/ *PIGZ*$^{PIG\text{-}Z}$			+	++	++	+++	++	+++	++++
Overexp Diap1									
NCBP2^{Cbp20}/ *Overexp Diap1*			+		++	+			
DLG1^{dlg1}/ *Overexp Diap1*			++			+++			

The number of "+" symbols indicate the severity of the observed cellular defects.

Table S7. Screening for interactions between 3q29 homologs and neurodevelopmental genes.

Second-hit gene	Cell cycle/ apoptosis	Microcephaly	$BDH1^{CG8888}$	$DLG1^{dlg1}$	$NCBP2^{Cbp20}$	$PAK2^{Pak}$
$ASPM^{asp}$	X	X	Enhancer (1/1)	No interaction (0/1)	Enhancer (1/1)	No interaction (0/1)
$CADPS2^{Cadps}$			Enhancer* (2/2)	No interaction (0/2)	Enhancer** (2/2)	Enhancer* (2/2)
$CENPJ^{Sas\text{-}4}$	X	X	Enhancer (2/2)	Not validated (1/2)	Enhancer (2/2)	No interaction (0/2)
$CHD8^{kis}$	X		No interaction (0/2)	Not validated (1/2)	Not validated (1/2)	No interaction (0/2)
$CHRNA7^{nAChR\alpha6}$ $CHRNA7^{nAChR\alpha7}$			Enhancer (3/5)	Enhancer (3/5)	Enhancer (3/5)	Enhancer (2/5)
$CTNNB1^{arm}$	X		Enhancer* (2/2)	Enhancer* (2/2)	Enhancer* (2/2)	Enhancer* (2/2)
$EPHA6^{Eph}$			Enhancer* (3/3)	Enhancer* (2/3)	Enhancer* (3/3)	Not validated (1/3)
$KIF11^{Klp61F}$	X	X	Enhancer (1/1)	Enhancer (1/1)	Enhancer (2/2)	Enhancer (1/1)
$LGR5^{rk}$	X		Enhancer (4/5)	No interaction (0/5)	Enhancer (4/5)	No interaction (0/5)
$MCPH1^{MCPH1}$	X	X	Enhancer (3/3)	No interaction (0/3)	Enhancer (2/3)	Not validated (1/3)
$NRXN1^{Nrx\text{-}1}$			Enhancer (3/3)	Not validated (1/3)	Enhancer (3/3)	No interaction (0/3)
$PTEN^{Pten}$	X		Enhancer** (2/2)	Enhancer* (2/2)	Enhancer** (2/2)	Not validated** (1/2)
$SCN1A^{para}$			Enhancer* (2/3)	No interaction (0/3)	Enhancer** (3/3)	Not validated (1/3)
$SHANK3^{Prosap}$			No interaction** (0/2)	No interaction** (0/2)	Not validated (1/2)	No interaction** (0/2)
$UBE3A^{Ube3a}$			Not validated** (1/2)	No interaction (0/2)	Enhancer** (2/2)	Not validated (1/2)
Lines tested (153)			38	38	39	38
All interactions (45/60)			13/15	8/15	15/15	9/15
Validated interactions (34/60)			12/15	5/15	13/15	4/15
Synergistic interactions (10/21)			3/7	1/4	4/6	2/4

"All interactions" indicates the number of crosses where a single two-hit line showed enhancement of the single-hit phenotype, while "Validated interactions" indicates the number of interactions which have at least a second cross with a validation line (if available) confirming the same result. "Synergistic interactions" indicates the number of interactions that exhibit synergistic effects (**) compared with those showing additive effects (*), as determined by two-way ANOVA tests (**Figure S7**). Shaded interactions indicate pairwise crosses where the 3q29 gene phenotype was not significantly enhanced, but the phenotype of the second-hit neurodevelopmental gene phenotype was suppressed. Second-hit neurodevelopmental genes are annotated for cell cycle/apoptosis function (Gene Ontology terms GO:0007049 and GO:0006915) as well as association with microcephaly disorders (7). We note that two fly homologs of *CHRNA7* were crossed with 3q29 genes, and their results were combined for the final counts.

Table S8. Pathogenicity metrics, animal model phenotypes, and biological functions of 3q29 genes.

3q29 gene	Pathogenicity metrics		Mouse phenotypes							Molecular function	Cell cycle/ apoptosis	Neuronal function
	RVIS %	pLI	Behavioral/ neurological	Cellular	Embryo	Growth/ size/body	Mortality/ aging	Nervous system	Other			
BDH1	76.70%	0.000								Ketone body metabolism enzyme localized in the mitochondrial membrane.		
CEP19	54.13%	0.053	X			X			X	Cilia assembly and microtubule anchoring at the centriole.		
DLG1	76.09%	0.999	X	X	X	X	X	X	X	Scaffolding protein involved with proliferation, signal transduction, synaptogenesis, and cell junction formation.	X	X
FBXO45	50.60%	0.858	X	X			X	X	X	E3 ubiquitin ligase complex subunit involved with neuromuscular synapse formation, axon guidance, and neuron migration.		X
LRRC33	15.35%	0.458		X					X	Transforming growth factor beta-1 regulator involved with microglia function and immune response.		
MFI2	46.54%	0.000								Cell-surface glycoprotein involved in iron uptake.		
NCBP2	48.98%	0.267	X				X		X	Cap binding complex protein and transcriptional regulator involved with mRNA splicing, nonsense-mediated decay, and nuclear transport.		
OSTalpha	26.73%	0.058				X			X	Solute carrier protein that transports bile acid from intestinal cells into the bloodstream.		
PAK2	29.64%	0.939		X	X	X	X	X	X	Involved in RAC1/Rho-GTPase and JNK signaling pathways that regulate cell cycle/growth, proliferation, apoptosis, cytoskeleton formation, and cell movement.	X	X
PCYT1A	10.99%	0.098			X		X		X	Enzyme for phosphatidylcholine synthesis.		
PIGX	79.65%	NA								Endoplasmic reticulum protein involved in GPI anchor synthesis (paralog of *PIGZ*).		
PIGZ	71.45%	0.000								Endoplasmic reticulum protein involved in GPI anchor synthesis (paralog of *PIGX*).		
RNF168	76.70%	0.000		X					X	E3 ubiquitin ligase protein involved in histone ubiquitination during DNA double-stranded break repair.		
SENP5	75.46%	0.996								Protease involved in SUMO protein regulation.	X	
SMCO1	88.52%	0.000								Unknown function.		

TCTEX1D2	70.81%	0.000							X	Cytoplasmic dynein subunit involved in intracellular motility, including ciliary, axonal, and organelle movement.		
TFRC	14.32%	0.780		X	X	X	X	X	X	Membrane receptor for cellular uptake of iron.		
TM4SF19	89.31%	0.014								L6 superfamily protein with unknown function.		
UBXN7	37.75%	0.991					X			Transcription factor binding protein that regulates ubiquitination of cullin ring ligases.		
WDR53	39.73%	0.000								Unknown function.		
ZDHHC19	90.85%	0.052								Zinc finger protein involved with palmitoyl transferase activity.		

3q29 genes with Residual Variation Intolerance Scores (RVIS) <20^{th} percentile (8) or probability of Loss-of-function Intolerant (pLI) scores >0.9 (9) are considered to be potentially pathogenic in humans and are shaded in gray. Mouse phenotypes for 3q29 genes were obtained from the Mouse Genome Informatics database (10). Molecular functions for 3q29 genes were derived from RefSeq, UniProtKB and Gene Ontology (GO) individual gene summaries (11–13), and annotations for cell cycle/apoptosis and neuronal function were derived from GO Biological Process annotations for each gene.

Table S9. List of candidate schizophrenia genes with apoptosis function (Excel file). This file lists 268 candidate schizophrenia genes that are annotated for apoptosis GO terms, including their membership within pathogenic CNVs.

Table S10. List of fly stocks for 3q29 homologs.

Gene name	Stock no.	Stock center	Genotype	Chrom.
BDH1^{CG8888}	30337	VDRC	w[1118]; P{GD3777}	2
DLG1^{dlg1}	41136	VDRC	w[1118];; P{GD4689}/TM3	3
FBXO45^{Fsn}	26577	VDRC	w[1118];; P{GD11383}	3
MFI2^{Tsf2}	5236	VDRC	w[1118];; P{GD2442}	3
NCBP2^{Cbp20}	107112	VDRC	y,w[1118]; P{KK109448}	2
OSTalpha^{CG6836}	108502	VDRC	y,w[1118]; P{KK112485}	2
PAK2^{Pak}	108937	VDRC	y,w[1118]; P{KK101874}	2
PCYT1A^{Pcyt2}	105794	VDRC	y,w[1118]; P{KK110819}	2
PIGX^{PIG-X}	101805	VDRC	y,w[1118]; P{KK109717}	2
PIGZ^{PIG-Z}	106747	VDRC	y,w[1118]; P{KK107404}	2
SENP5^{Ulp1}	31744	VDRC	w[1118];; P{GD7581}	3
TCTEX1D2^{CG5359}	104357	VDRC	y,w[1118]; P{KK107839}	2
UBXN7^{CG8892}	28985	VDRC	w[1118]; P{GD14061}	2
WDR53^{CG5543}	106320	VDRC	y,w[1118]; P{KK109031}	2
ZDHHC19^{app}	106488	VDRC	y,w[1118]; P{KK108227}	2
Validation lines				
Gene name	**Stock no.**	**Stock center**	**Genotype**	**Chrom.**
BDH1$^{CG8888(EY12413)}$	21078	BDSC	y[1] w[67c23]; P{w[+mC] y[+mDint2]=EPgy2}CG8888[EY12413]	2
BDH1$^{CG8888(MI13104)}$	58023	BDSC	y[1] w[*]; Mi{y[+mDint2]=MIC}CG8888[MI13104]	2
BDH1$^{CG8888(KK\_RNAi)}$	110467	VDRC	y,w[1118]; P{KK101971}	2
DLG1$^{dlg1(KK\_RNAi)}$	109274	VDRC	y,w[1118]; P{KK116285}	2
DLG1$^{dlg1(5)}$	36280	BDSC	dlg1[5]/FM7a	1
FBXO45$^{Fsn(KG08128)}$	14562	BDSC	y[1]; P{y[+mDint2] w[BR.E.BR]=SUPor-P}Fsn[KG08128]/CyO; ry[506]	2
FBXO45$^{Fsn(TRiP)}$	31096	BDSC	y[1] v[1]; P{y[+t7.7] v[+t1.8]=TRiP.JF01561}attP2	3
MFI2$^{Tsf2(KG01571)}$	13452	BDSC	y[1]; P{y[+mDint2] w[BR.E.BR]=SUPor-P}Tsf2[KG01571] ry[506]/TM3, Sb[1] Ser[1]	1
NCBP2$^{Cbp20(TRiP)}$	42596	BDSC	y[1] sc[*] v[1]; P{y[+t7.7] v[+t1.8]=TRiP.HMS02428}attP40	2
NCBP2$^{Cbp20(GD\_RNAi)}$	50433	VDRC	w[1118];; P{GD17252}/TM3	3
PAK2$^{Pak(11)}$	8810	BDSC	Pak[11]/TM3, Sb[1]	3
PAK2$^{Pak(6)}$	8809	BDSC	Pak[6]/TM3, Sb[1] Ser[1]	3
PIGZ$^{PIG-Z(TRiP)}$	38360	BDSC	y[1] sc[*] v[1]; P{y[+t7.7] v[+t1.8]=TRiP.HMS01828}attP2	3
SENP5$^{Ulp1(KK\_RNAi)}$	106625	VDRC	y,w[1118]; P{KK107062}	2
WDR53$^{CG5543(GD\_RNAi)}$	27454	VDRC	w[1118]; P{GD11687}	2

This table lists the stock lines, stock center, and genotypes for primary and validation 3q29 homolog lines. BDSC: Bloomington *Drosophila* Stock Center; VDRC: Vienna *Drosophila* Resource Center.

Table S11. List of fly stocks for other neurodevelopmental genes.

Gene name	Stock no.	Stock center	Genotype	Chrom.
$ASPM^{asp\_2}$	2911	VDRC	w[1118]; P{GD1375}	2
$CADPS2^{Cadps}$	25291	VDRC	w[1118]; P{GD9502}	2
$CADPS2^{Cadps\_2}$	25292	VDRC	w[1118];;P{GD9502}	3
$CENPJ^{Sas\text{-}4}$	106051	VDRC	y,w[1118]; P{KK100878}	2
$CENPJ^{Sas\text{-}4\_2}$	17975	VDRC	w[1118]; P{GD6852}	2
$CHD8^{kis}$	46685	VDRC	w[1118]; P{GD16331}	2
$CHD8^{kis\_2}$	109414	VDRC	y,w[1118]; P{KK100890}	2
$CHRNA7^{nAChR\alpha6}$	101571	VDRC	y,w[1118]; P{KK103877}	2
$CHRNA7^{nAChR\alpha6\_2}$	8889	VDRC	w[1118]; P{GD1045}	2
$CHRNA7^{nAChR\alpha6\_3}$	8890	VDRC	w[1118];; P{GD1045}	3
$CHRNA7^{nAChR\alpha7}$	100756	VDRC	y,w[1118]; P{KK108471}	2
$CHRNA7^{nAChR\alpha7\_2}$	11329	VDRC	w[1118];; P{GD3742}	3
$CTNNB1^{arm}$	7767	VDRC	w[1118];; P{GD1372}	3
$CTNNB1^{arm\_2}$	107344	VDRC	y,w[1118]; P{KK102545}	2
$EPHA6^{Eph}$	6545	VDRC	w[1118] P{GD39}	1
$EPHA6^{Eph\_2}$	27236	VDRC	w[1118]; P{GD14481}	2
$EPHA6^{Eph\_3}$	4771	VDRC	w[1118];; P{GD2535}	3
$KIF11^{Klp61F}$	52548	VDRC	w[1118]; P{GD14149}	2
$KIF11^{Klp61F\_2}$	52549	VDRC	w[1118];; P{GD14149}	3
$LGR5^{rk}$	105360	VDRC	y,w[1118]; P{KK108009}	2
$LGR5^{rk\_2}$	904	VDRC	w[1118];; P{GD15}	3
$LGR5^{rk\_3}$	4753	VDRC	w[1118];; P{GD12774}	3
$LGR5^{rk\_4}$	29931	VDRC	w[1118]; P{GD14383}	2
$LGR5^{rk\_5}$	29932	VDRC	w[1118];; P{GD14383}	3
$MCPH1^{MCPH1}$	28098	VDRC	w[1118]; P{GD12537}	2
$MCPH1^{MCPH1\_2}$	28100	VDRC	w[1118]; P{GD12537}	2
$MCPH1^{MCPH1\_4}$	21066	VDRC	w[1118];; P{GD9974}	3
$NRXN1^{Nrx\text{-}1}$	4306	VDRC	w[1118]; P{GD2619}	2
$NRXN1^{Nrx\text{-}1\_2}$	36328	VDRC	w[1118]; P{GD14451}	2
$NRXN1^{Nrx\text{-}1\_3}$	36326	VDRC	w[1118];; P{GD14451}/TM3	3
$PTEN^{Pten}$	101475	VDRC	y,w[1118]; P{KK109278}	2
$PTEN^{Pten\_2}$	35731	VDRC	w[1118];; P{GD13500}	3
$SCN1A^{para}$	104775	VDRC	y,w[1118]; P{KK108534}	2
$SCN1A^{para\_2}$	6131	VDRC	w[1118];; P{GD3392}	3
$SCN1A^{para\_3}$	6132	VDRC	w[1118];; P{GD3392}/TM3	3
$SHANK3^{Prosap}$	103592	VDRC	y,w[1118]; P{KK101537}	2
$SHANK3^{Prosap\_2}$	21218	VDRC	w[1118];; P{GD10101}/TM3	3
$UBE3A^{Ube3a}$	100130	VDRC	y,w[1118]; P{KK104898}	2
$UBE3A^{Ube3a\_2}$	45876	VDRC	w[1118]; P{GD450}	2
UAS-Diap1	6657	BDSC	w[*]; P{w[+mC]=UAS-DIAP1.H}3	3
UAS-Dronc	56758	BDSC	w[*]; P{w[+mC]=UAS-Dronc.EGFP}3	3

This table lists the stock lines, stock center, and genotypes for neurodevelopmental and apoptosis genes outside of the 3q29 region used in two-hit experiments. BDSC: Bloomington *Drosophila* Stock Center; VDRC: Vienna *Drosophila* Resource Center.

Table S12. Statistical analysis of experimental data (Excel file). This file shows all statistical information (statistical test and controls used, test statistics, p-values, confidence intervals, ANOVA factors/degrees of freedom, and sample size) for the data presented in the main and supplemental figures.

Table S13. Morpholinos used for *X. laevis* experiments.

Gene	Morpholino
NCBP2	for L, 5'- CGGTTTCCCTAGAATAGAAACAGGT-3'
FBXO45	for L and S, 5'-TATCTGTGGTGGGAAGAAAAGGTCA-3'
DLG1	for L, 5'-CAAATGAGGCAGCAACTTACTTTCT-3'
PAK2	for L and S, 5'-AGAGATAAATCCTACCTTTTTCTGT-3'
standard control	5′-cctcttacctcagttacaatttata-3′

Table S14. qPCR primers used for *X. laevis* experiments.

Gene	Primers
NCBP2	forward for L allele 5'- ATCTGAGTCAGTATCGGGACC-3' reverse for L allele 5'- CCCTTCCTTAAATCCTGCATCC-3'
FBXO45	forward for L and S allele 5'- CCGACATACTGTGCAACCTG-3' reverse for L and S allele 5'-TGTCCAAGATCACCCGAATCC-3'
DLG1	forward for L allele 5'-CTCTCCTATGAACCCGTCAC-3' reverse for L allele 5'-CCGGCCTCTATGAATTTGTG-3'
PAK2	forward for L and S allele 5'-AGGATAAACCACCAGCTCCTC-3' reverse for L and S allele 5'-GGGAGCCCATCTTTATCTGGTG-3'
ODC1 control	forward 5'- GCCATTGTGAAGACTCTCTCCATTC-3' reverse 5'- TTCGGGTGATTCCTTGCCAC-3'

Video S1. Negative geotaxis experiments for single-hit knockdowns. This video shows the climbing ability of control, $NCBP2^{Cbp20}$ and $DLG1^{dlg1}$ individual knockdown flies at day 10 of the negative geotaxis experiments.

Video S2. Negative geotaxis experiments for two-hit knockdowns. This video shows the climbing ability of $NCBP2^{Cbp20}/DLG1^{dlg1}$ and $NCBP2^{Cbp20}/FBXO45^{Fsn}$ pairwise knockdown flies at day 10 of the negative geotaxis experiments.

References

1. Iyer J, et al. (2016) Quantitative Assessment of Eye Phenotypes for Functional Genetic Studies Using Drosophila melanogaster. *G3 (Bethesda)* 6(5):1427–1437.

2. Greenwood S, Struhl G (1999) Progression of the morphogenetic furrow in the Drosophila eye: the roles of Hedgehog, Decapentaplegic and the Raf pathway. *Development* 126(24):5795–808.

3. Hu Y, et al. (2011) An integrative approach to ortholog prediction for disease-focused and other functional studies. *BMC Bioinformatics* 12(1):357.

4. Chintapalli VR, Wang J, Dow JAT (2007) Using FlyAtlas to identify better Drosophila melanogaster models of human disease. *Nat Genet* 39(6):715–720.

5. Graveley BR, et al. (2011) The developmental transcriptome of Drosophila melanogaster. *Nature* 471(7339):473–479.

6. Green EW, Fedele G, Giorgini F, Kyriacou CP (2014) A Drosophila RNAi collection is subject to dominant phenotypic effects. *Nat Methods* 11(3):222–3.

7. Nicholas AK, et al. (2009) The molecular landscape of ASPM mutations in primary microcephaly. *J Med Genet* 46(4):249–53.

8. Petrovski S, Wang Q, Heinzen EL, Allen AS, Goldstein DB (2013) Genic Intolerance to Functional Variation and the Interpretation of Personal Genomes. *PLoS Genet* 9(8):e1003709.

9. Lek M, et al. (2016) Analysis of protein-coding genetic variation in 60,706 humans. *Nature* 536(7616):285–291.

10. Smith CL, et al. (2018) Mouse Genome Database (MGD)-2018: knowledgebase for the laboratory mouse. *Nucleic Acids Res* 46(D1):D836–D842.

11. O’Leary NA, et al. (2016) Reference sequence (RefSeq) database at NCBI: current status, taxonomic expansion, and functional annotation. *Nucleic Acids Res* 44(D1):D733-45.

12. UniProt Consortium (2018) UniProt: the universal protein knowledgebase. *Nucleic Acids Res* 46(5):2699–2699.

13. The Gene Ontology Consortium (2019) The Gene Ontology Resource: 20 years and still GOing strong. *Nucleic Acids Res* 47(D1):D330–D338.